APTAMER ENCODED NANOPORES AS SINGLE MOLECULE SENSORS

A Thesis Presented to

The Faculty of the Graduate School

University of Missouri

In Partial Fulfillment

Of the Requirements for the Degree

Master of Science

---

by

SHU DING

Dr. Li-Qun (Andrew) Gu, Thesis Supervisor

DECEMBER 2008

The undersigned, appointed by the Dean of the Graduate School, have examined the thesis entitled

APTAMER ENCODED NANOPORES AS SINGLE MOLECULE SENSORS

Presented by Shu Ding

A candidate for the degree of Master of Science

And hereby certify that in their opinion it is worthy of acceptance.

_____

Li-Qun (Andrew) Gu, Ph.D., Biological Engineering

_____

Jinglu Tan, Ph.D., Biological Engineering

_____

Fu-Hung Hsieh, Ph.D., Biological Engineering

_____

Gabor Forgacs, Ph.D., Physics

ACKNOWLEDGEMENTS

I would like to thank my lab group for supporting me on this project. My supervisor, Dr. Li-Qun (Andrew) Gu, Dr. Changlu Gao, Mr. Qiulin Tan and Dr. Jiwook Shim are the lab members that helped me.

I am grateful to my committee members: Dr. Jinglu Tan, Dr. Fu-Hung Hsieh, and Dr. Gabor Forgacs. They gave me suggestions and advised me in my research.

I owe a special note of thanks to my father, Xiaoning Ding, mother, Zhimei Wang, and my beloved husband Jiexuan He for their support.

TABLE OF CONTENTS

LIST OF FIGURES

LIST OF TABLES

APTAMER ENCODED NANOPORES AS SINGLE MOLECULE SENSORS

Shu Ding

Dr. Li-Qun (Andrew) Gu, Thesis Supervisor

ABSTRACT

We have created a low noise, calibrated, molecular-scaled pore. The nanopore is formed either by micro-forge polishing or external penetration of the nanocavity sealed in the pipette terminal. The nanopore fabrication is both cost-effective and time-efficient. The uniform profile of the nanocavity is imaged by a scanning electron microscope (SEM). It suggested a molecular scale pore size and conical pore shape. By correlating pore size and conductance, we have established a method for calibrating pore size by conductance level. The pore diameter was further verified by the translocation of double-strand DNA (dsDNA), which has a known size ~2nm.

Our study shows that glass nanopore can be modified with DNA/RNA aptamer as a promising biosensor. Single molecules (IgE, Ricin and streptavidin/biotin) were detected rapidly and sensitively in real time electrical measurement. Simultaneous recording showed a dynamic process in molecule recognition and interaction. This demonstrated that a glass nanopore could impact single protein molecule detection for medical and biothreat applications.

One of the exciting observations is a single restriction enzyme (*Hind*III) activity within nano-confinement. The duration of event could indicate the strength of the interaction and the amplitude of the event could indicate different protein conformations. We demonstrated the ability of a functionalized nanopore to measure the recognition and interaction on a single molecule scale. It can provide deeper insight and understanding of the stochastic interaction of various biomolecules.

CHAPTER 1

INTRODUCTION

In cell membranes, single nanometer-sized pores (nanopores) control the essential part of ions and molecules transported in and out of the cell. Advanced nanotechnology now allows an artificial nanopore to be fabricated on solid-state substrates. It provides a new class of nanosensors for rapid electrical detection of single molecules.

1.1 Biological nanopores

Alpha-haemolysin (Song et al., 1996) is a transmembrane protein which spontaneously inserts into a lipid membrane and forms a nanopore (Fig. 1.1). Negative charged ssDNA can be driven into the Alpha-haemolysin by an electric field (Kasianowicz et al., 1996). But the double-strand DNA (dsDNA) cannot enter the nanopore, since its diameter (~2nm) is wider than the narrowest entrance of Alpha-haemolysin (1.4nm). When the ssDNA passes through the nanopore like a thread through a needle eye, the ionic current is partial blocked. The reduced current amplitude recovers until the ssDNA exits. Thus, the single ssDNA translocation event is detected by the Alpha-haemolysin pore (Fig. 1.2).

Figure 1.1. The cross-sectional structure of α-haemolysin (Song et al., 1996).

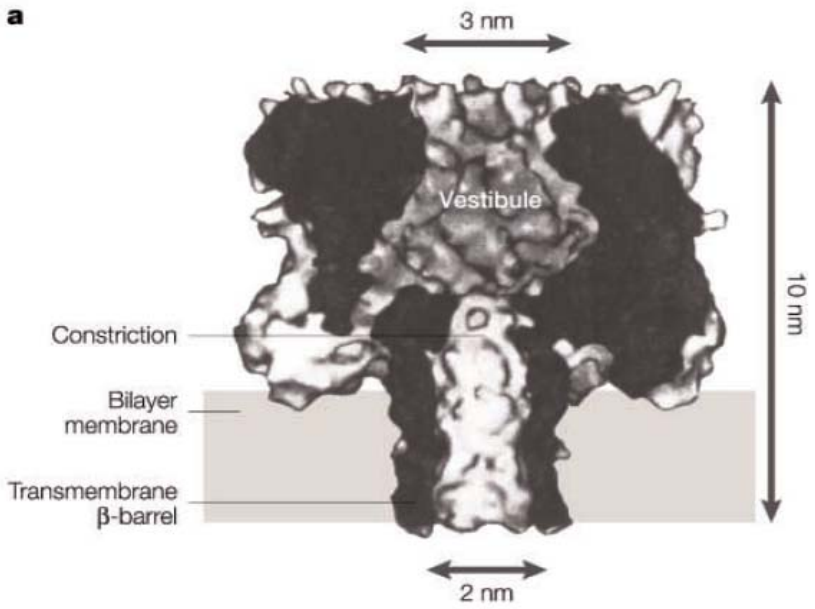

Figure 1.2. A ssDNA molecules passing through α-haemolysin (Dekker 2007).

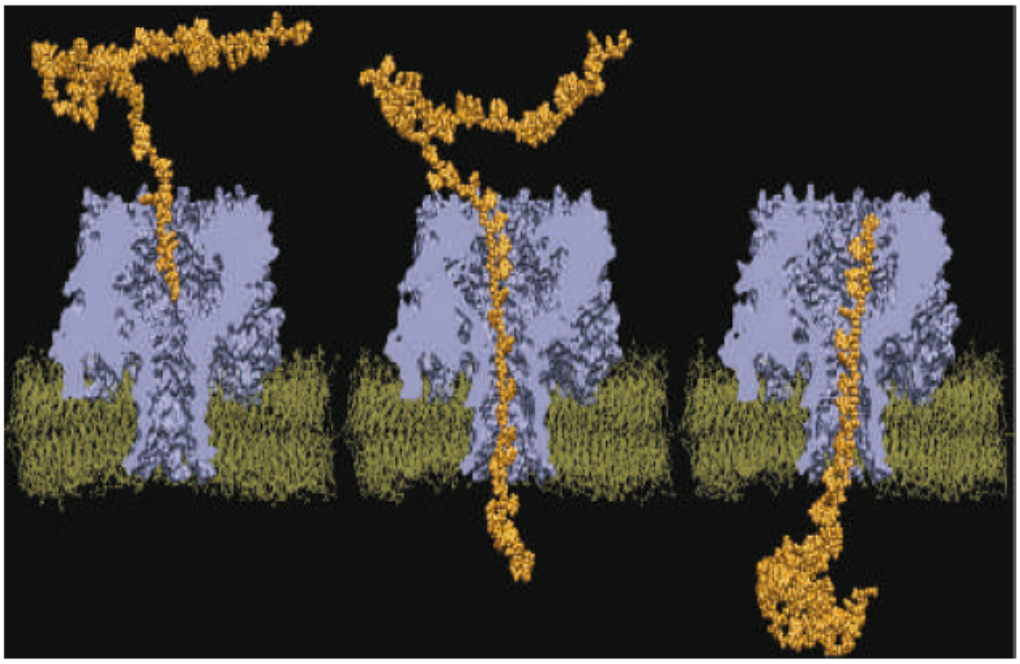

A good advantage of biological nanopores is that they can be developed through structure-directed genetic engineering and chemical modification. For example, by attaching a nucleotide oligomer probe at a specific site, sequence-specific individual DNA strands can be detected (Howorka et al., 2001). In the past few years, it has been suggested that the nanopore can be used as a device for DNA sequencing (Fig. 1.3).

Figure 1.3. A single-base mismatch detection in DNA-nanopore (Howorka et al., 2001).

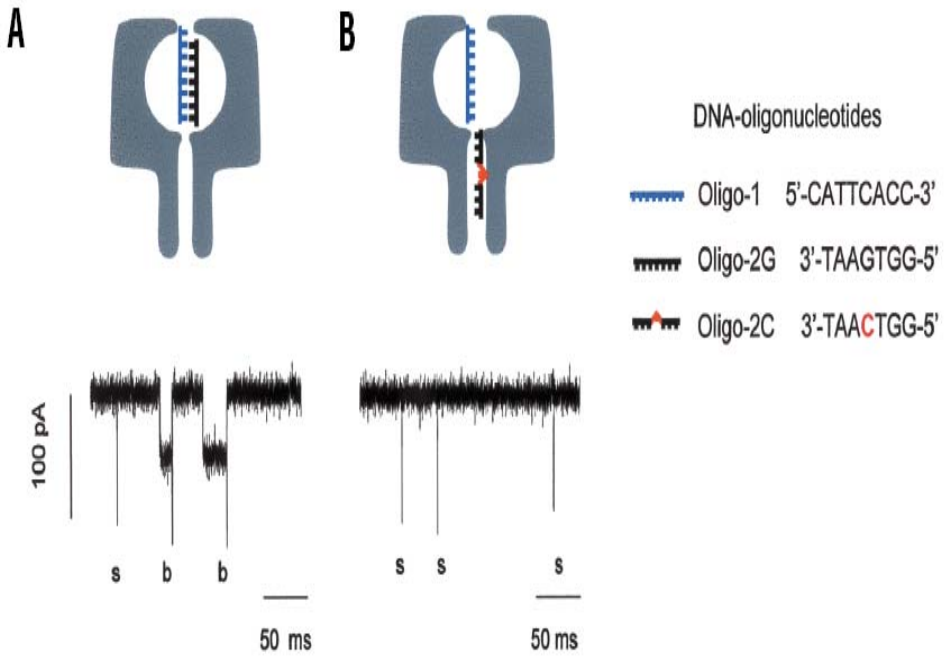

However, the biological nanopores are limited by a fixed pore size and by the fragile lipid bilayer in which the pore is embedded. It becomes unstable when the external environment changes, such as electrical voltage, salt concentration, pH and/or temperature.

1.2 Solid-state nanopores

Nanotechnology provides sophisticated tools for constructing a variety of solid-state nanopores which have advantages over biological nanopores, such as controllable pore size and high stability.

The challenge is to fabricate pores in solid materials with nanometer dimensions. The first reported single nanopores (Li et al., 2001) were fabricated by "sculpting" with a focused ion beam on thin Si_3N_4 membranes (Fig. 1.4). Using a transmission electron microscope (TEM), another type of nanopore (Storm et al., 2003) was developed in a silicon membrane (Fig. 1.5). However, these methods require expensive instruments and well-trained operators. Another well-established method involves creating a polymer film nanopore through ion-track etching. The dimension of this internally-etched pore can be controlled by the etching conditions. However, this method requires special materials, such as a polymer film with low-density ion tracks. The glass micropipette requires no special equipment or techniques. It can be precisely pulled to form a narrow conduit on its terminal. The glass pore can be made as small as tens of nanometers, and have potential uses in controlled delivery, ion conductance microscopes, and nanosensor and DNA sequencing. However, the glass nanopore is limited by the difficulty in controlling the pore size.

Figure 1.4. Solid-state nanopore on Si_3N_4 membrane sculpted by focused ion beam technique (Li et al., 2001).

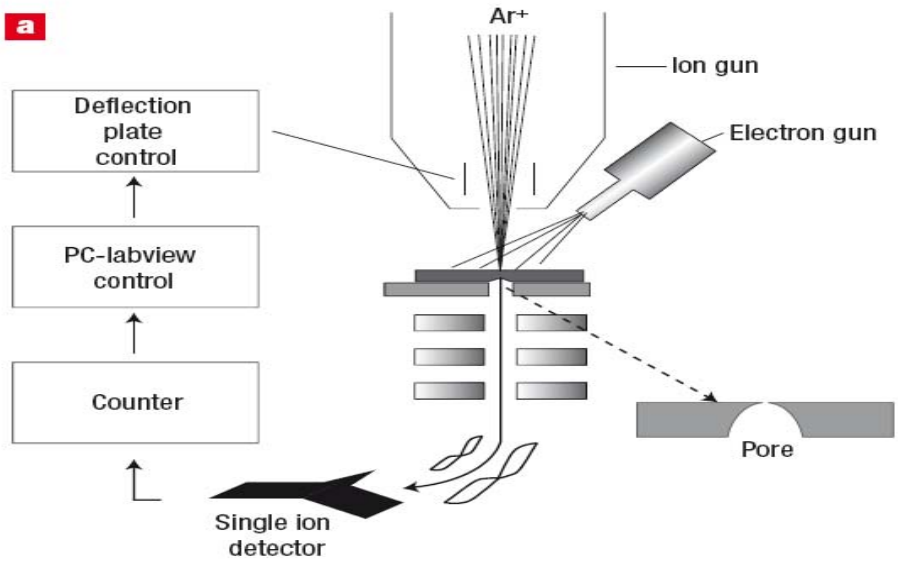

Figure 1.5. Solid-state nanopore on SiO_2 membrane fabricated by TEM technique (Storm et al., 2003).

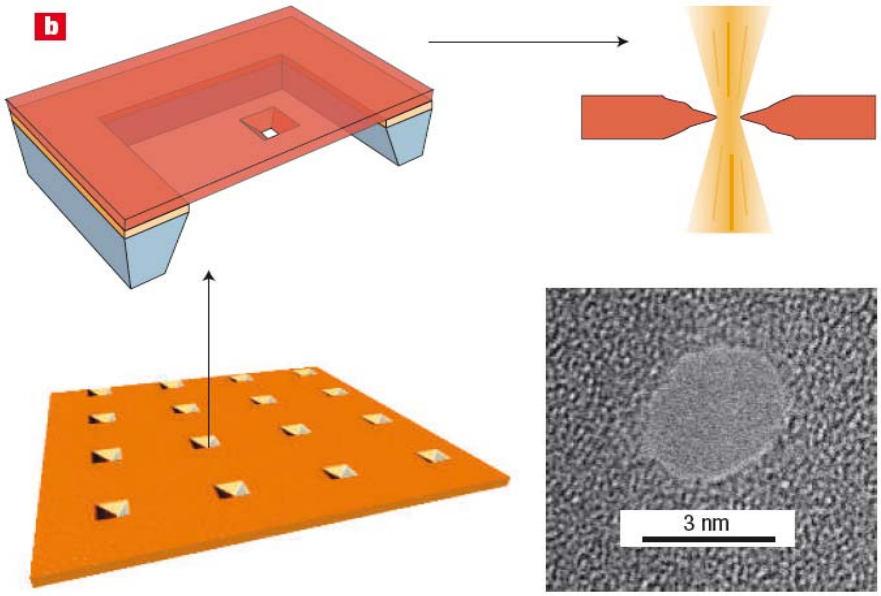

Similar to biological nanopores, single molecule translocaion was also detected by solid-state nanopores. Because of the variability of pore sizes, not only ssDNA but also dsDNA were able to pass through the nanopore (Storm et al., 2005). Using the electrical measurement, the stochastic molecule translocation was able to be monitored (Fig. 1.6). Each spike indicated a single dsDNA traverses the nanopore. It contains abundant important information in each single molecule translocation event. For example, by analyzing the amplitude and duration of current blockage, different types of translocations were distinguished for different lengths of dsDNA (Storm et al., 2005), and therefore made this solid-state nanopore a possible candidate for DNA sizing.

Figure 1.6. dsDNA translocation through solid-state nanopores (Storm et al., 2005).

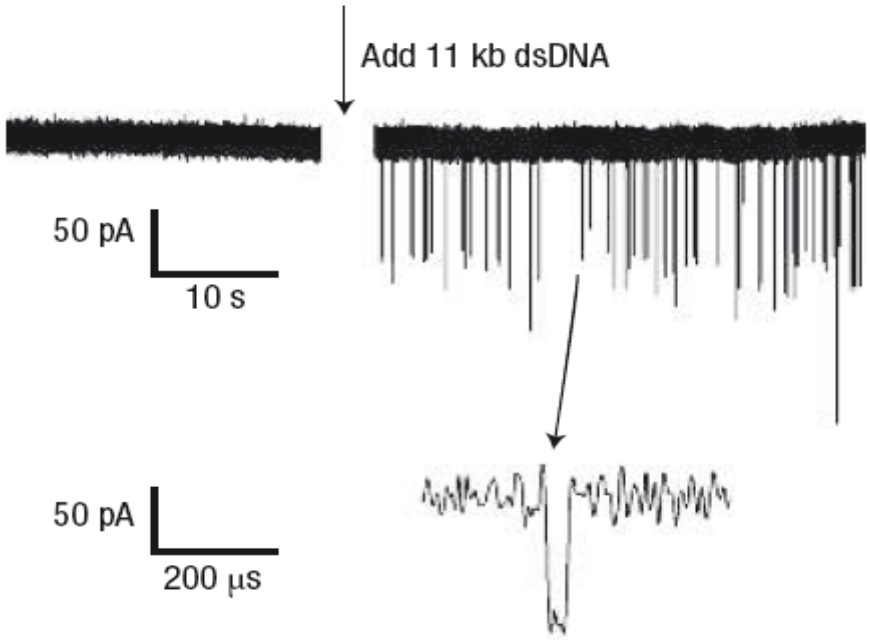

Because solid-state nanopores are stable in a wide range of solutions and environments, it can be engineered as a potential device for DNA sequencing (Samir et al., 2007). Single-base mismatch was able to be identified in DNA-functionalized nanopores (Fig. 1.7).

Figure 1.7. Solid-state nanopore channels with DNA selectivity (Samir et al., 2007).

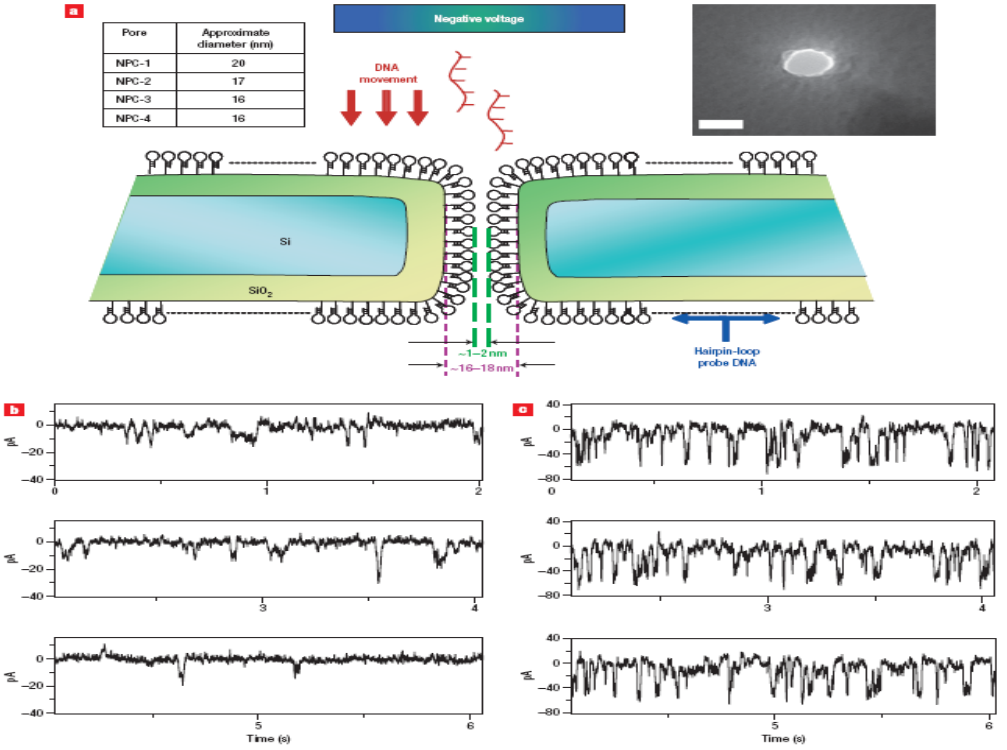

Mismatched DNA Perfect-complementary DNA

Although the field of solid-state nanopores rapidly growing, it's still young. Many questions remain unsolved. For example, the fabrication process, which is not consistent, results in a large variance in the pore diameter. A significant noise is also undesirable.

We have discovered a much more efficient process for creating a low-noise nanopore at the molecular level on the terminal of a silica capillary pipette. More importantly, we were able to establish a method for calibrating the pore size by controlling the level of pore conductance. This robust nanopore can be made as small as 1nm so that a single molecule of cyclodextrin can be trapped in the pore, offering new nanopore functions such as chiral-discrimination (Gao et al., 2008).

CHAPTER 2

NANOPORE FABRICATION

Objective

To create or fabricate a nanopore embedded in a glass membrane with a single nanometer precision.

Methods

2.1 Nanopore fabrication method I: simple heat polishing process

In a typical patch-clamp experiment, the tip of the pipette is heat polished to remove the surface irregularities and to provide a smooth tip. We used this simple process to create a nanometer sized pipette tip. The diameter was precisely shrinked from a micrometer scale to a nanometer scale until it formed a single nanopore embedded in a glass membrane.

Figure 2.1. CPM-2 Microforge (Dr. Kevin Gillis lab, University of Missouri).

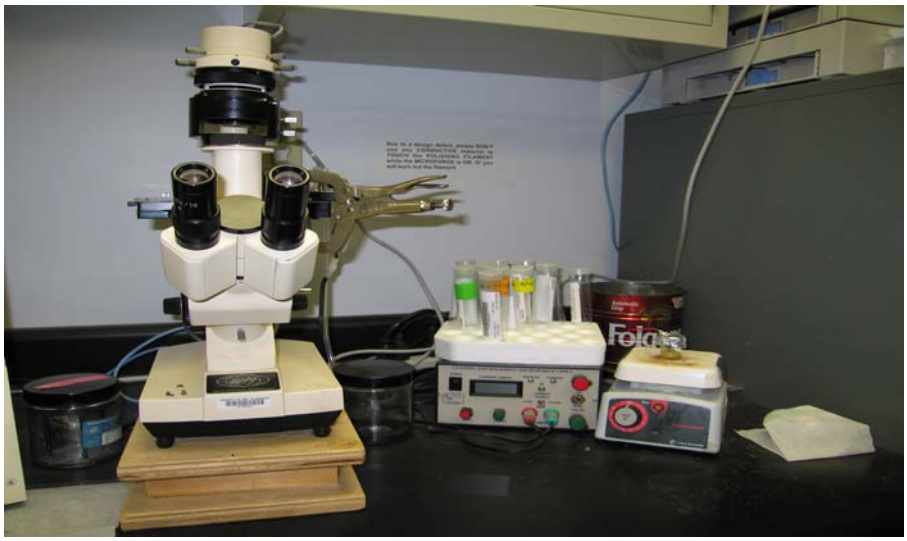

The microforge works with an inverted microscope (World Precision Instrument PIM-R), under which the pipette tip can be observed (Fig. 2.1). The polishing filament is placed in front of the pipette tip (Fig. 2.1). As the given power increases, it generates heat. When the heat reaches the pipette tip, the glass surface tension is reduced. So the local glass material melts and the pipette tip diameter shrinks. We controlled the power, heating time and heat distance from the pipette tip to the polishing filament. When the heat is stopped, a pipette tip with a nanometer scale is obtained.

Figure 2.2. Nanopore fabrication by micro-forge.

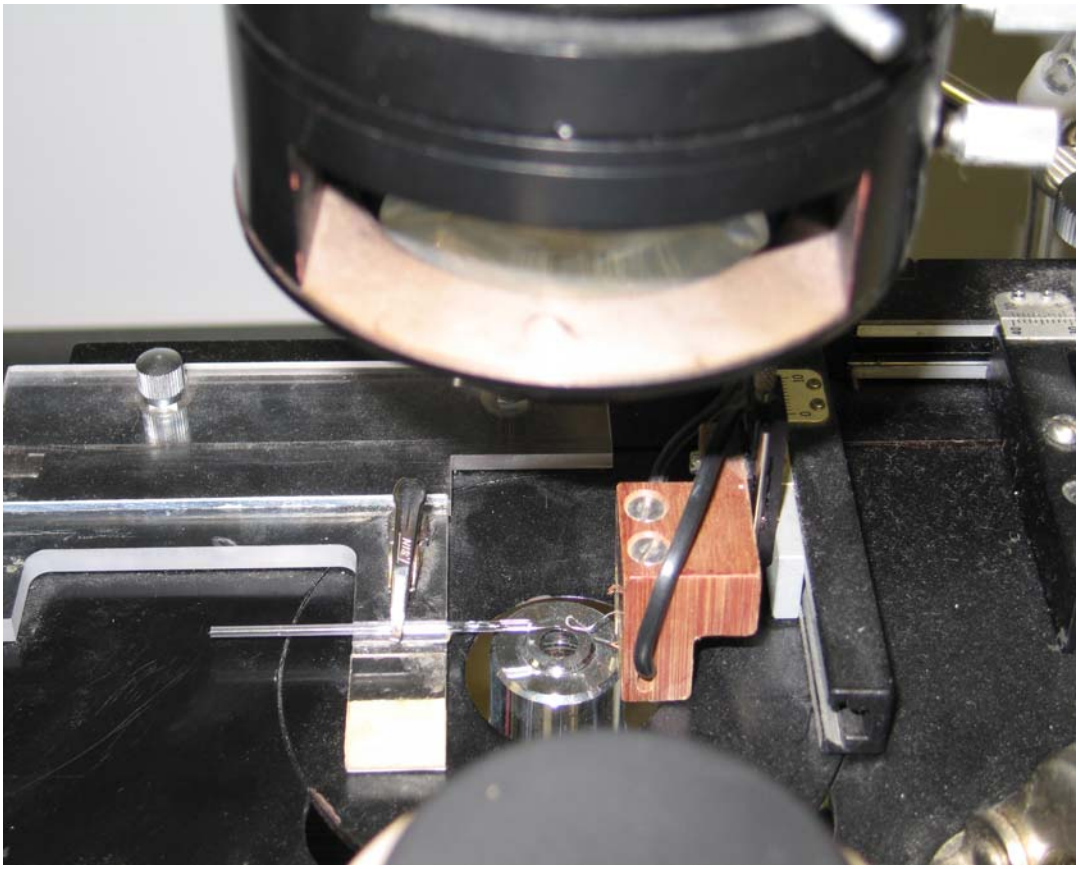

2.2 Fabrication method II: wet etching

Another type of nanopore can be fabricated by the wet etching method. Controlled by the etching rate and etching time, the nanopore size can increase from small to large. In contrast to the microforge method, we formed a closed pipette tip first. Then we used etchant (40% NH_4F/49% HF) to penetrate through the glass material from the outside of the pipette tip. As the surrounding glass material was gradually removed, a single nanopore embedded in a pipette tip was exposed (Fig. 2.3).

Figure 2.3. Nanopore fabricated by the wet etching method.

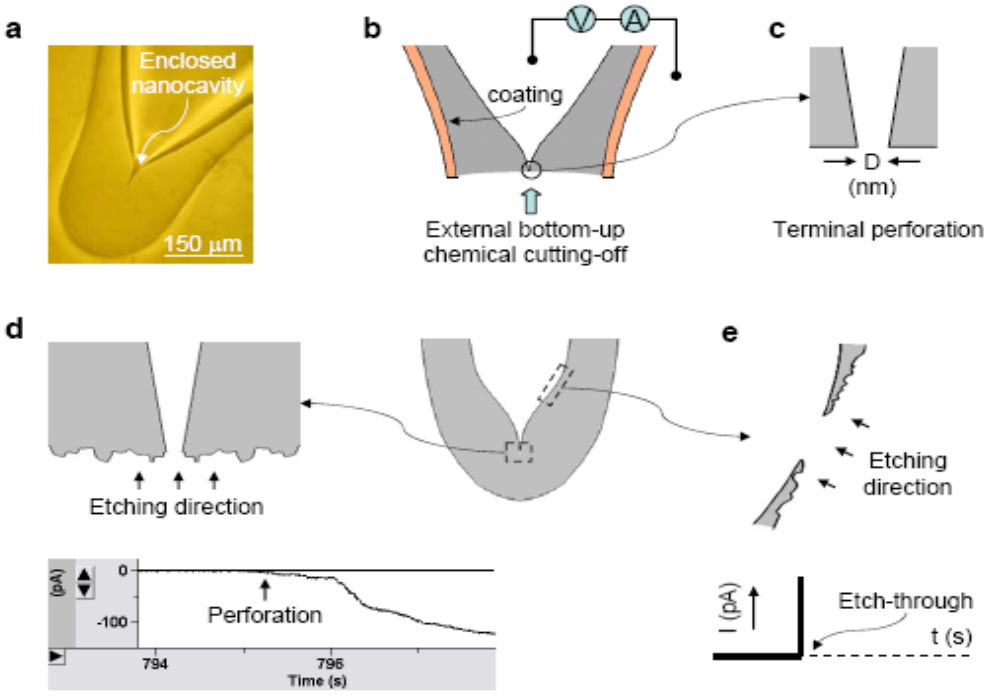

Before use, the borosilicate glass tube (1.5 mm o.d. and 0.86 mm i.d.) with an inner filament (A-M System Inc.) was washed with ethanol and double deionized water (ddH2O), followed by drying in nitrogen air.

The cleaned tube was heated to around 400ºC for 1 hr in a furnace to improve surface smoothness. The processed tube was pulled into two micropipettes using a laser puller (Sutter Inc). The narrow tip was melted with a micro-forge setup until the terminal was completely closed and a 100 μm spherical tip was formed (Fig. 2.3a). The tube was then filled with the solution containing 1 M NaCl and 10 mM Tris (pH7.5). The inner filament assisted in delivering the solution to the closed end. The terminal was also examined under an optical microscope to ensure that no air bubble was isolated inside.

Next, the narrow terminal was coated with a protective layer of orthodontic wax (Sunstar Americas) or SU-8 Resists (MicroChem). Other coating materials that resist etching can also be used. The coating thickness is not important. The wax was completely melted before being applied. The terminal was quickly tip-dipped in the wax solution. The SU-8-covered terminal was soft-baked at 90°C for 10 minutes for solidification. After it was thoroughly cured, the coating on the bottom of the terminal was carefully removed, allowing the local silica surface to be accessible to the chemical solution for bottom-up etching (Fig. 2.3b). The terminal was immersed in a solution of 40% NH4F/49% HF for etching. The etching procedure was monitored through two Ag/AgCl electrodes spanning the solutions inside and outside the glass tube. Once the terminal was perforated from the bottom (Fig. 2.3c), as identified by the gradually increasing current (Fig. 2.3d, bottom panel), it was immediately washed with 50 mM NaOH for 1-5 seconds to neutralize the etched surface, followed by washing with

ddH2O. It was then quickly transferred to a 1 M NaCl solution, the same solution as inside the pipette, for measuring conductance.

Results

2.3 SEM images of nanopores created by method I: micro-forge

The glass nanopore diameter was precisely shrunk from the initial dimension of approximately 500nm to 20nm. The changes in pore diameter can be monitored using a scanning electron microscope. The smallest nanopore we have observed is about 20nm (Fig. 2.4). Due to the limitation of the SEM resolution, we couldn't get a sharp image of the nanopore with a diameter smaller than 20nm.

Figure 2.4. A sequence of a nanopore image using Scanning Electron Microscope. Nanopore diameter shrinks gradually from 500nm to about 20nm.

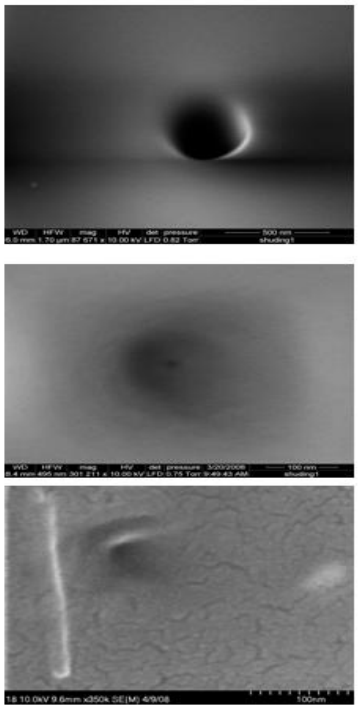

Diameter ~ 500nm

Diameter ~ 100nm

Diameter ~ 20nm

2.4 SEM image of nanopores created by method II: wet etching

In principle, the glass nanopores diameter was able to grow from small to large under a finely controlled etching rate and etching time. But it's hard to observe a nanopore directly, because the glass surface was chemically damaged by etching. It's not smooth and clear enough to find a small pore in a large surface area. To assess the pore size and shape, we used this glass nanopore as a template to form a polymer nanowire, which was then imaged by a scanning electron microscope. According to the product instruction book, the two components of the silicone elastomer polydimethylsiloxane (PDMS, SylgardR 184, Dow Corning) were mixed and vacuumed to remove the bubbles. The liquid PDMS was then injected into the micropipette, followed by spinning in a microcentrifuge at 10,000 rpm for 2 minutes to deliver the polymer to the nanopore. After curing at 90^0C for 4 hours, the glass tube was carefully removed manually and a PDMS nanocone was exposed for imaging. Before the SEM imaging, the nanowire was coated with a layer of platinum.

Figure 2.5. A SEM image of PDMS nanocone formed from nanopore template.

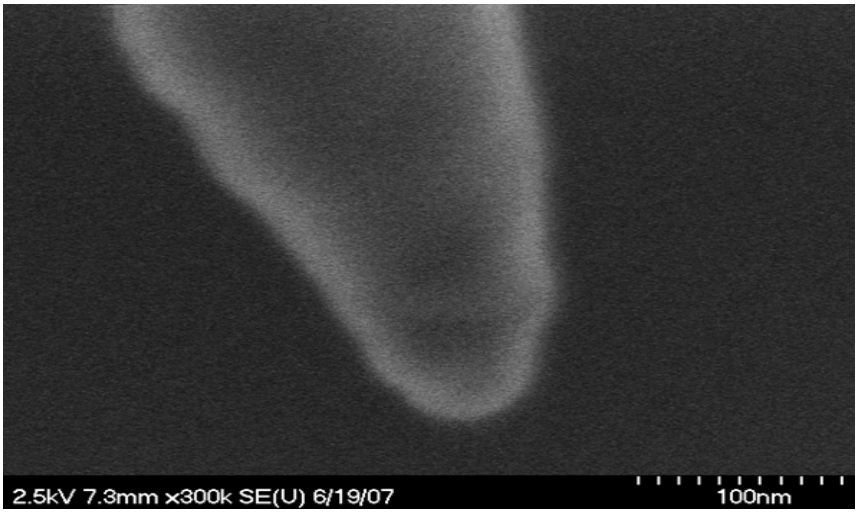

The image from the scanning electron microscope showed a conical-shaped nanowire with an aperture of ~30° and terminal diameter of ~50 nm (Fig. 2.5). However, this image did not clearly reveal the geometry at the very end of the nanowire.

Conclusions

Through standard pulling, forging and external etching processes, we can create nanopores of various pore sizes from a uniform nanocavity sealed in the pipette terminal. The fabrication is simple, requiring no special or expensive equipment. The nanopore can be made using resources available in laboratories at all levels. Nanopores with sizes from 20nm to 500nm were imaged. However, a pore with a diameter smaller than 20nm was hard to observe directly under the scanning electron microscope.

CHAPTER 3

CALIBRATION OF NANOPORE SIZE

Objective

To evaluate pore diameters by electrical measurement of pore conductance, especially for the small diameter which is unable to be observed directly under the scanning electron microscope. To establish a relationship between the nanopore diameter and conductance.

Methods

Pico-ampere electrical recording (Fig. 3.1). The Conductance was measured in 1M NaCl solution using an Axopatch 200B-2 patch-clamp amplifier (Molecular Device Inc.), then low-pass filtered with a built-in 4-pole Bessel filter at 1-5 kHz and sampled at 5-10 kHz with a Digidata 1332 A/D converter (Molecular Device Inc.). For all measurements, the external solution was grounded as the convention for voltage polarity.

Figure 3.1. Pico-ampere electrical recording.

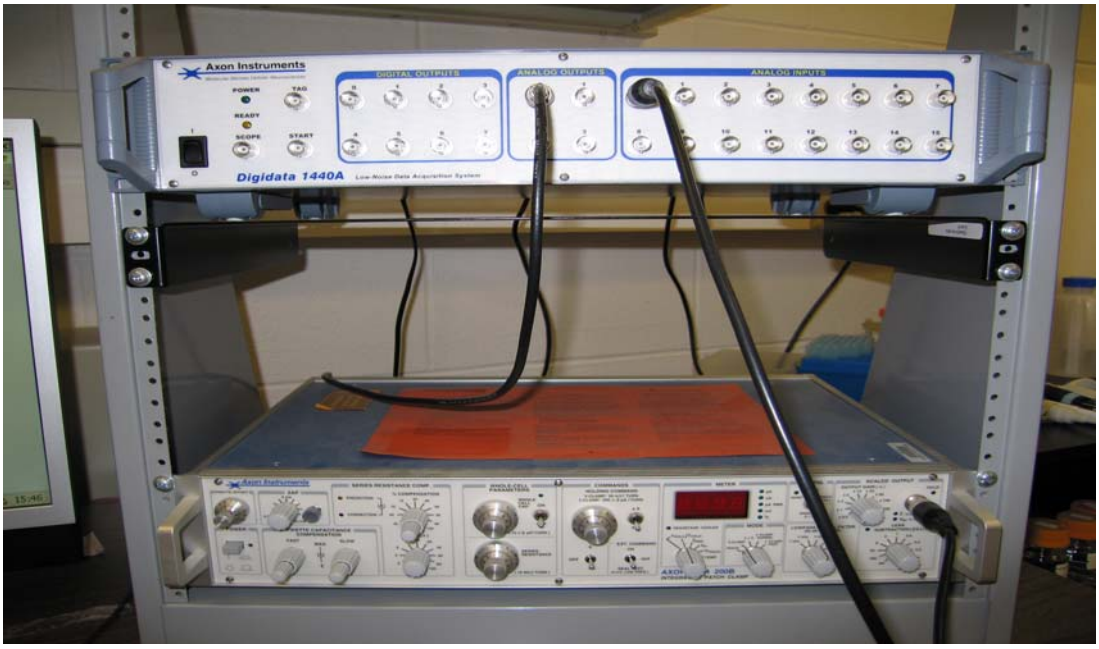

Results

3.1 Pore diameter and conductance relationship

3.1.1 Nanopore created by method I: micro-forge

Constructed by a micro-forge method in a heating time series, the nanopore diameter was measured directly using the scanning electron microscope. A relationship between the pore diameter and conductance (50mV, 1M NaCl) was established as in Table 3.1.

Table 3.1. A relationship between the pore size and conductance.

Pore diameter (nm)	Pore conductance (nS)
5000	75000
1000	6180
600	5320
500	1260
400	316
300	164
250	150
200	140
100	40
50	6

3.1.2 The conductance of nanopore created by method II: wet etching

In the absence of a SEM image, we measured the pore conductance (20mV 1M NaCl pH = 7.0) corresponding to the etching time (Table 3.2).

Table 3.2. A relationship between the etching time and pore conductance. Etching solution: 40% NH_4F : 49% HF = 30 :1 (v/v), etching speed: 0.63 nm/s (25^{o}C).

Etching time (sec)	Average pore conductance (nS)
0	0
5	1.2
10	3.9
15	5.3
20	7.5
25	9.4
35	36.5
45	66.5
55	117.5
65	172.5
75	233.5
85	301.0
95	367.0
105	565.0
115	645.0
125	762.0
135	800.0
145	874.5
155	1030.0
165	1120.0
175	1210.0
185	1280.0

3.2 dsDNA translocation to assess the small pore size

It was difficult to observe our nanopores under the electron microscope. One reason is its much smaller pore size (~102 nm^2 in cross area) compared to the 108-fold larger terminal ball surface (104 μm^2). The chemically damaged glass surface after etching is another obstacle for imaging. In the following experiments, we focused on the study of etched nanopores.

In the absence of direct microscopic observation, the translocation of analytes of known dimension can help reveal the pore size. Briefly, a molecule narrower than the nanopore could pass through the pore, but a molecule wider than the pore could not. A single molecule traversing a nanopore with the appropriate pore size will block the pore current, producing an electrical signature that can be used to identify the molecular translocation, and thereby, the pore size. This method of pore size assessment has been shown to be valid in many nanopore detections. For example, dsDNA with a known size has been used to probe the lumen profile and the dimension of solid-state pores (Storm et al., 2005).

We observed the translocation of dsDNA (~2 nm) in the glass nanopore, although the pore size remains unknown (Fig. 3.2). A 10nM of 1 kbp dsDNA was presented in the external solution. A positive voltage should drive the negatively-charged DNA into the nanopore. The current block was not detected for a low conductance nanopore, but began to appear after the conductance was raised to 3.8 nS (Fig. 3.2a and b). At this conductance level, the average block duration, τ, was 1.5 seconds, and the block occurrence, f, was 0.21 min-1 at +100 mV. Because the purified DNA was the only macromolecular component in the solution, we attributed these blocks to the linear DNA

traversing the pore. After the current recording, we collected 10 μl of the internal solution (around the nanopore) for the polymer chain reaction (PCR), assuming that the amplified DNA would be detected if a DNA translocation occurred. The PCR target was a 350 bases fragment. The agarose gel (Fig. 3.2c) revealed PCR products. Lane-2 showed a thick DNA band for the external solution containing DNA, and Lane-3 showed no band for the internal solution without DNA. Both Lane-2 and Lane-3 were control tests. The band of the amplified DNA for the internal solution after the electrical detection was identified in Lane-4 (same position as in Lane-2), verifying the existence of DNA in the internal solution that had traveled from the external bath through the nanopore. The large signal in Lane-4 could be a result of long time recording. The number of dsDNA translocated into the nanopore is large after several hours. We ran another PCR experiment (Fig. 3.3) to show the difference between the short-time and long-time recording.

Figure 3.2. dsDNA translocation events though glass nanopores.

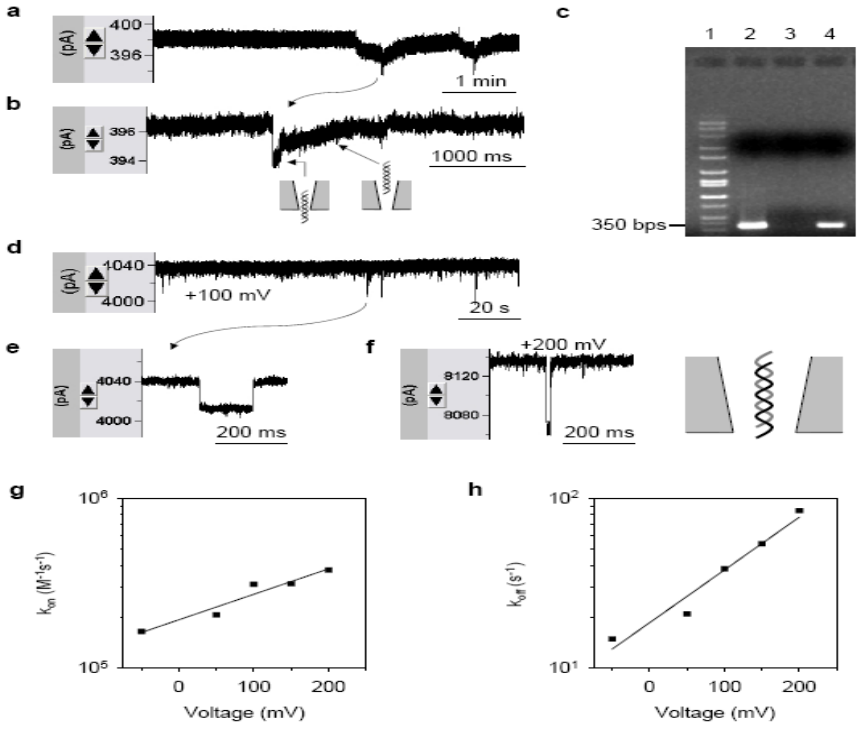

Figure 3.3. PCR results showing the difference in recording times (10 vs. 100 mins).

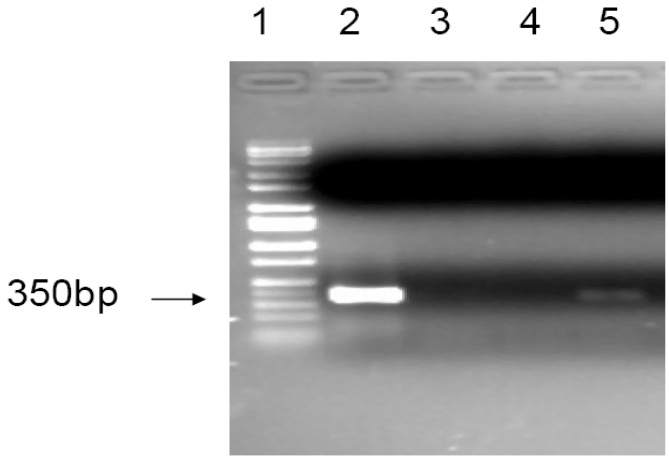

Lane-1 marker, Lane-2 external dsDNA solution (10nM), Lane-3 internal solution before recording (1M NaCl), Lane-4 internal solution after short time recording (10 mins), lane-5 internal solution after long time recording (100 mins).

As pore conductance increased, the blockage was shortened and occurred more frequently. For a 39 nS pore, τ was 26 ms and f was 1.9 min^{-1} at +100 mV (Fig. 3.2d and e). Since 3.8 nS (Fig. 3.2a) was the lowest pore conductance required for dsDNA translocation, we inferred a pore size comparable to the dimension of dsDNA (2 nm). Due to the negative charge on DNA molecules, the DNA translocation was also influenced by the voltage. For example, the 39 nS pore recorded at +200 mV, τ was shortened to 12 ms (Fig. 3.2f) and f, increased to 2.1 min^{-1}. Fig. 2g and h illustrates the voltage-enhanced translocation rate constant (kon) and the rate constant for DNA escape from the nanopore (koff). Due to the negative charge, the DNA translocation was also verified by the voltage-dependence of block duration and occurrence. Fig. 3.2g showes the decreased of block duration and Fig. 3.2h shows the increased of block occurrence as the voltage increased from -50 mV to +200 mV. The DNA translocation observed at low negative voltage (-50 mV) could be a joint effect of the diffusion, the weak electrical force that prevents DNA from entering the pore, and the electroosmotic force that drives molecules into the pore.

The DNA translocation at a pore size comparable to the dimension of the DNA molecule produces a novel block profile (Fig. 3.2b) different from the typical rectangular block in a larger nanopore (Fig. 3.2e). Because DNA translocation is slowed at this pore size, the block profile can reveal sequential steps in a translocation event (Fig. 3.2b). The initial current drop marks a single DNA molecule entering the pore. The ensuing recovering current corresponds to the DNA threading the conical-shaped lumen and escaping from the pore into the pipette. In addition, the amplitude of the current blockage in the 3.8 nS pore (~2pA) was smaller than in the 39 nS pore (~30 pA).

Earlier studies have shown that the duration of DNA translocation varies from ~50 μs to ~100 ms, depending on both properties of nanopore and DNA (Table 3.3). For example, the duration of a 0.5 kb dsDNA traversing a 5 nm Si_3N_4 pore (10 nm in length) at +120 mV was 5 ms (Li et al., 2001), and that for a 7.5 kb dsDNA through a 40 nm polymer conical pore at +700 mV was 100 ms (Harrell et al., 2006). By comparison, the 26 ms block duration in our 39 nS pore (Fig. 3.2b) is consistent with this time scale. However, the 1.5 s duration in the 3.8 nS pore (Fig. 3.2a) is longer than this range. A possible explanation is that the pore size at the threshold conductance is comparable to the dimension of dsDNA (2 nm), thus the traversing speed is slowed down probably due to a stronger DNA-pore interaction. The block profile in the nanopore at the threshold conductance (Fig. 3.2a) was also different from the typical rectangular block in a larger nanopore (Fig. 3.2b), revealing sequential steps involved in a translocation event (model in Fig. 3.2a); the initial current drop marks the moment when a DNA is entering the pore. The ensuing recovering current corresponds to the DNA threading the conical-shaped lumen and escaping from the wide opening of the pore into the pipette. It is noticed that the current amplitude of DNA block in the threshold conductance pore (~2 pA, Fig. 3.2a) is very small, compared with that in the wider pore (~30 pA, Fig. 3.2b). The variation of block conductance has been studied previously. The first discovery is that DNA translocation can increase, rather than decrease the pore conductance at 100 mM KCl (Chang et al., 2004). The reported results suggest that it is possible to observe a small conductance change upon DNA translocation under specific conditions. To interpret this phenomenon, an interfacial cation flow (I_{int}) between DNA and nanopore has been introduced that can compensate for the current loss from the DNA block. As we

observed the small block current at a pore size comparable to the DNA dimension, it is worth investigating in the future how the pore size, in addition to the ion concentration, affects the I_{int} component.

Table 3.3. Comparison of different types of solid-state nanopores.

Reference	Pore size (Diameter×Length)	DNA length	Voltage	Duration
Nanopore in this report	~9 nm (estimated from conductance)	1.0 kb	100 mV	26 ms
	~2 nm (at threshold conductance)	1.0 kb	100 mV	1.5 s
Li et al. (2001)	5 nm×10 nm	0.5 kb	120 mV	5 ms
Storm et al. (2005)	10 nm×20 nm	11.5 kb	120 mV	0.292 ms
		48.5 kb	120 mV	1.96 ms
Harrell et al. (2006)	40 nm tip of conical-pore	7.3 kb	700 mV	~100 ms

Conclusions

We demonstrated that a nanopore can be fabricated using a micro-forge or wet etching method. The nanopore diameter can either shrink or increase with a nanometer precision. The nanopore was visualized using a Scanning Electron Microscope. The nanopore surface and diameter were observed directly. The pore shape was indirectly revealed by a PDMS nanocone formed from a nanopore template. Due to the limitation of SEM resolution, we didn't get a sharp image showing the diameter is less than 20nm. Instead, we measured the pore conductance corresponding to the pore size. In addition, we used dsDNA as a molecule scale to show the capability of making a solid-state nanopore in a single molecular dimension.

CHAPTER 4

SINGLE MOLECULE DETECTION

IN APTAMER ENCODED NANOPORES

Objective

Using DNA/RNA aptamers as molecule receptors, to develop a sensor based on glass nanopore for rapidly and sensitively detecting analytes (IgE and Ricin) at the single molecule level.

Methods

4.1 Nanopore functionalization with DNA/RNA aptamers

Glass pipettes were cleaned for 30 min in 1M NaOH at 100^{o}C, followed by HCl (5%) for 5 min. The glass pipettes were then washed by DI water and dried for 30 min at 100^{o}C. We added a 90% methanol/water solution containing 2% aldehyde methoxysilane into the pipette for 3 hours. Then the pipettes were washed 5 times with 90% methanol/water, 5 times water and baked for 30 min at 100^{o}C. Silanized pipettes were incubated in a PBS solution (with 15mM NaN_3, PH7.4), containing 2μM 3'-amino-modified ssDNA aptamer and 2mM $NaBH_3CN$ overnight at room temperature. DNA Aptamer coated pipettes were washed by 1M NaCl and ready for the next test of single molecule detection.

4.2 Single molecule detection and electrical measurement

Aptamer coated nanopores were washed and filled with 1M NaCl. Current was measured by an amplifier and digidata 1440A (Axon Instruments) with 1M NaCl solution under 50mV. Then the NaCl solution was washed out and replaced by PBS (pH 7.4). Analytes, IgE (5nM), IgG (5nM) and IgE-aptamer complex (5nM) were added to the inside of the pipette. The ionic current was analyzed by Clampex 10.0.

Results

4.3 Nanopores modified with DNA/RNA aptamers

An aptamer (http://www.archemix.com/website/science_aptamer.php) is a nucleic acid macromolecule that binds tightly to a specific molecular target. Like all nucleic acids, a particular aptamer may be described by a linear sequence of nucleotides (A, U, T, C and G), typically 15-40 nucleotides long. In solution, the chain of nucleotides forms intermolecular interactions that fold the molecule into a complex three-dimensional shape (Cho et al., 2006). The shape of the aptamer allows it to bind tightly against the surface of its target molecule. (Fig. 4.1)

Firure 4.1. A 3-D structure showing an aptamer binding with its target. Anti-IgE aptamer has a hair-loop structure (Cho et al., 2006).

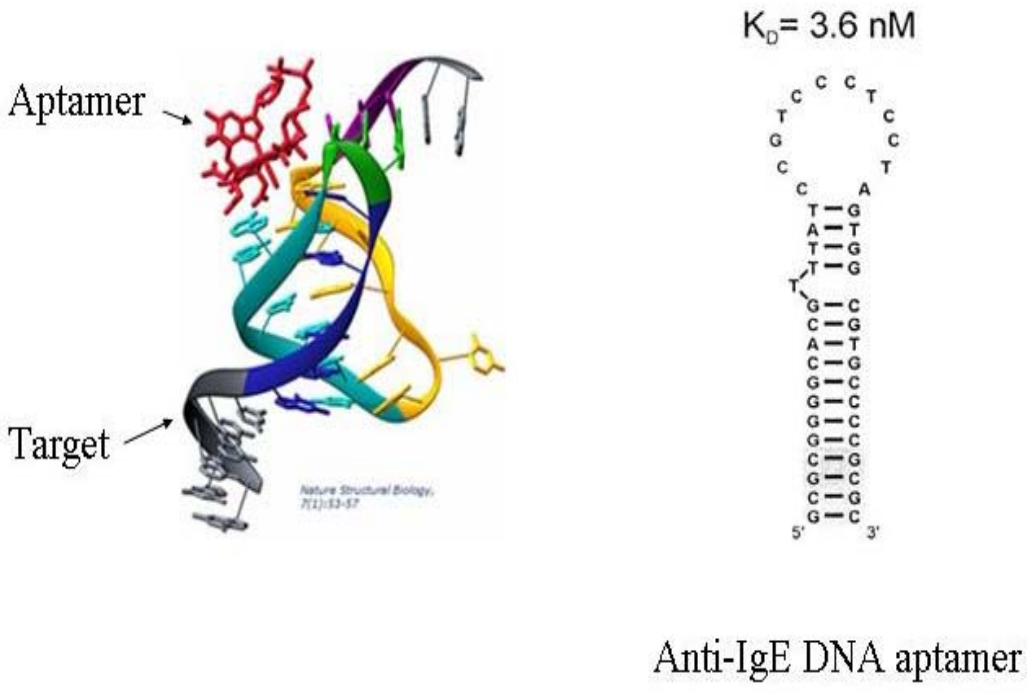

In addition to exhibiting remarkable specificity, aptamers generally bind their targets with a very high affinity. A survey of over 150 reported aptamers to a wide variety of targets reveal that the majority of anti-protein aptamers have equilibrium dissociation constants (Kds) in the picomolar (pM) to low nanomolar (nM) range.

More specifically, aptamers can be classified as DNA or RNA aptamers. They consist of (usually short) strands of oligonucleotides. Peptide aptamers consist of a short variable peptide domain, attached at both ends to a protein scaffold.

To functionalize nanopores as a biosensor, we modified the lumen surface of the nanopore with DNA/RNA aptamers. We selected aptamers as a molecule recognition agent because of the high affinity between aptamers and specific targets. DNA/RNA

aptamers were immobilized on a glass surface through an amino group (Stadther et al., 2005). A reducing agent, NaBH3CN, was used to enhance the coupling efficiency of aptamers to the glass surface (Fig. 4.2).

Figure 4.2. DNA aptamers covalently attached to the glass surface (Stadther et al., 2005).

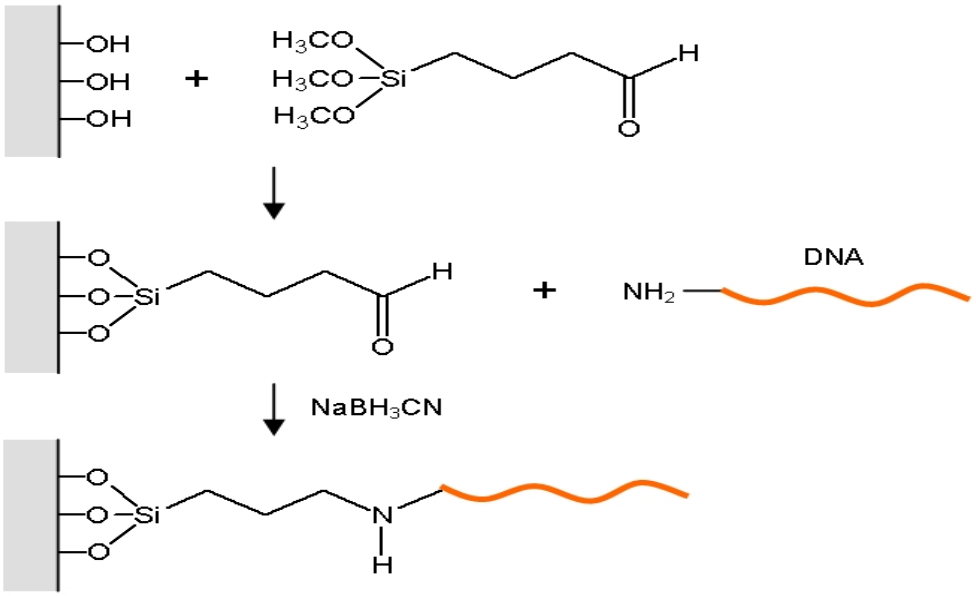

We compared the current after aptamer coating and noticed that it has a small reduction in current amplitude (Fig. 4.3). One possible reason is that aptamers partially block the ionic current. The steady state current is stable and low noise, which is suitable for detecting any small current signal changes caused by molecule recognition in the nanopore. The pore size is not critical for single-molecule detection.

Figure 4.3. Ionic current before and after DNA aptamer modification.

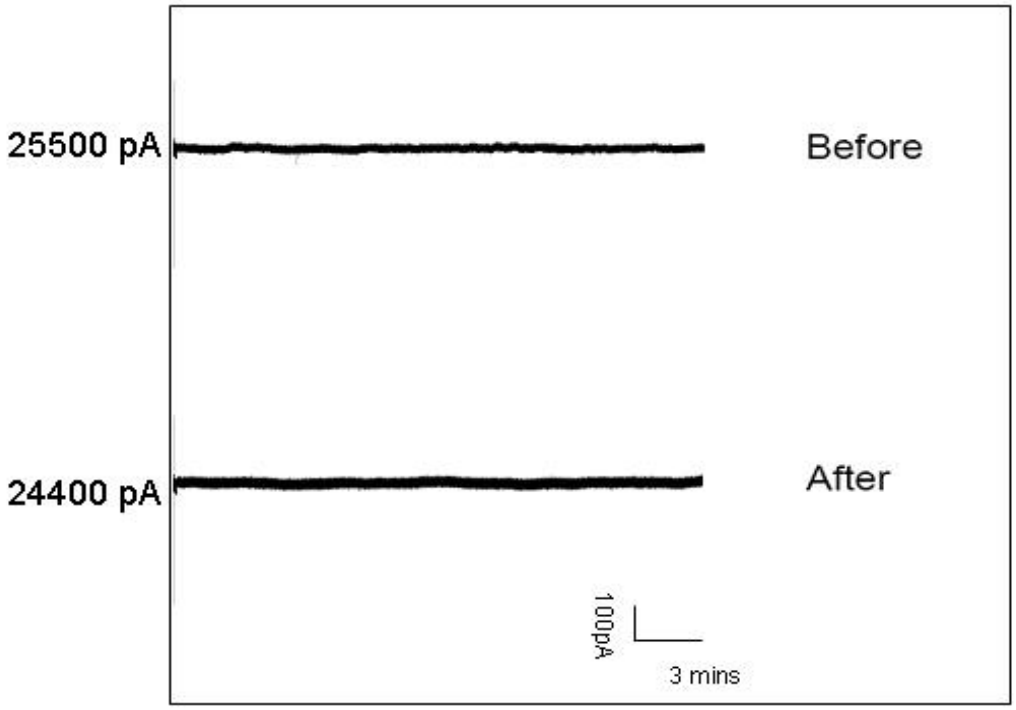

4.4 Single immunoglobulin E (IgE) detection

In biology, Immunoglobulin E (IgE) is a class of antibody that has only been found in mammals (Fig. 4.4). It plays an important role in allergies (Gould 2003). A person who has an allergy usually has elevated blood levels of IgE. IgE antibodies attack and engage the invading army of allergens. Immunoglobulin E (IgE) is one of the body's 5 classes (isotypes) of immunoglobulins (antibodies). Like other immunoglobulins, IgE is produced by B cells and plasma cells. In contrast to other immunoglobulins, the concentration of IgE in the circulation is very low. However, it is capable of triggering the most powerful immune reactions.

Figure 4.4. IgE structure (Gould 2003).

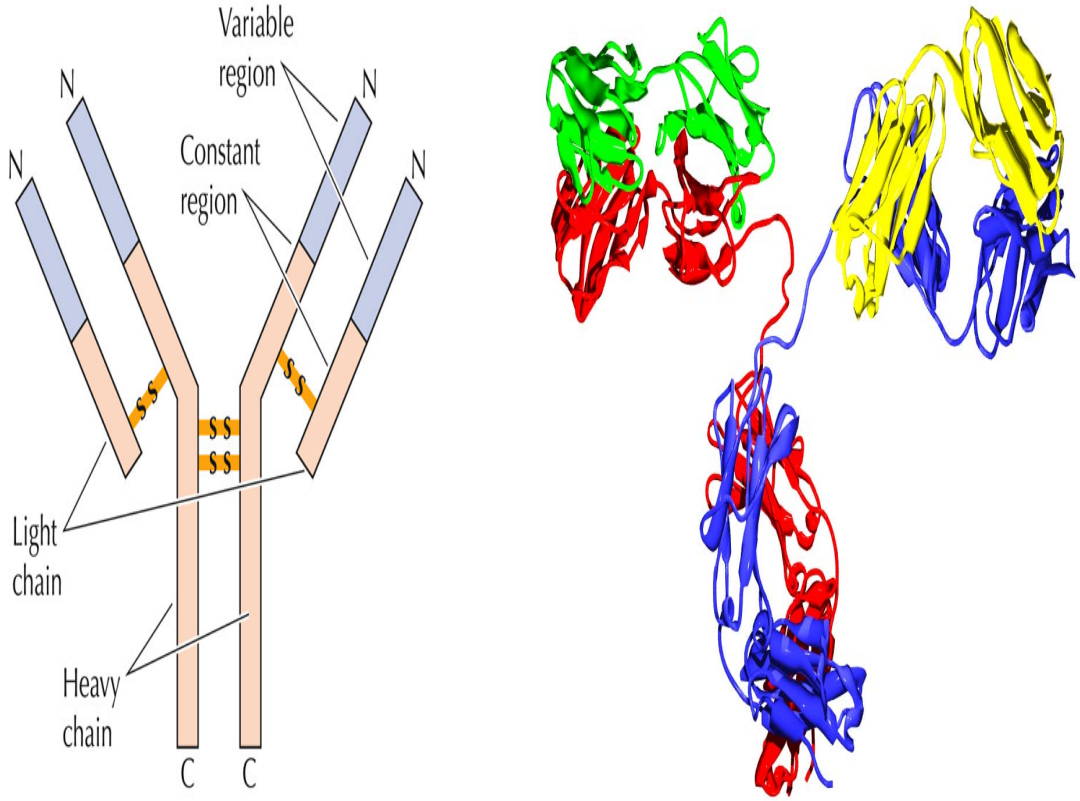

The concept of our experiment is illustrated schematically in Fig. 4.5: when an IgE molecule binds to an aptamer receptor on the lumen surface of the nanopore, the current should change from the base line. When more and more IgE molecules bind to the aptamer, the current drops in discrete steps.

Figure 4.5. Nanopore-based detection of IgE molecule. When IgE bind to the aptamer, the current should change.

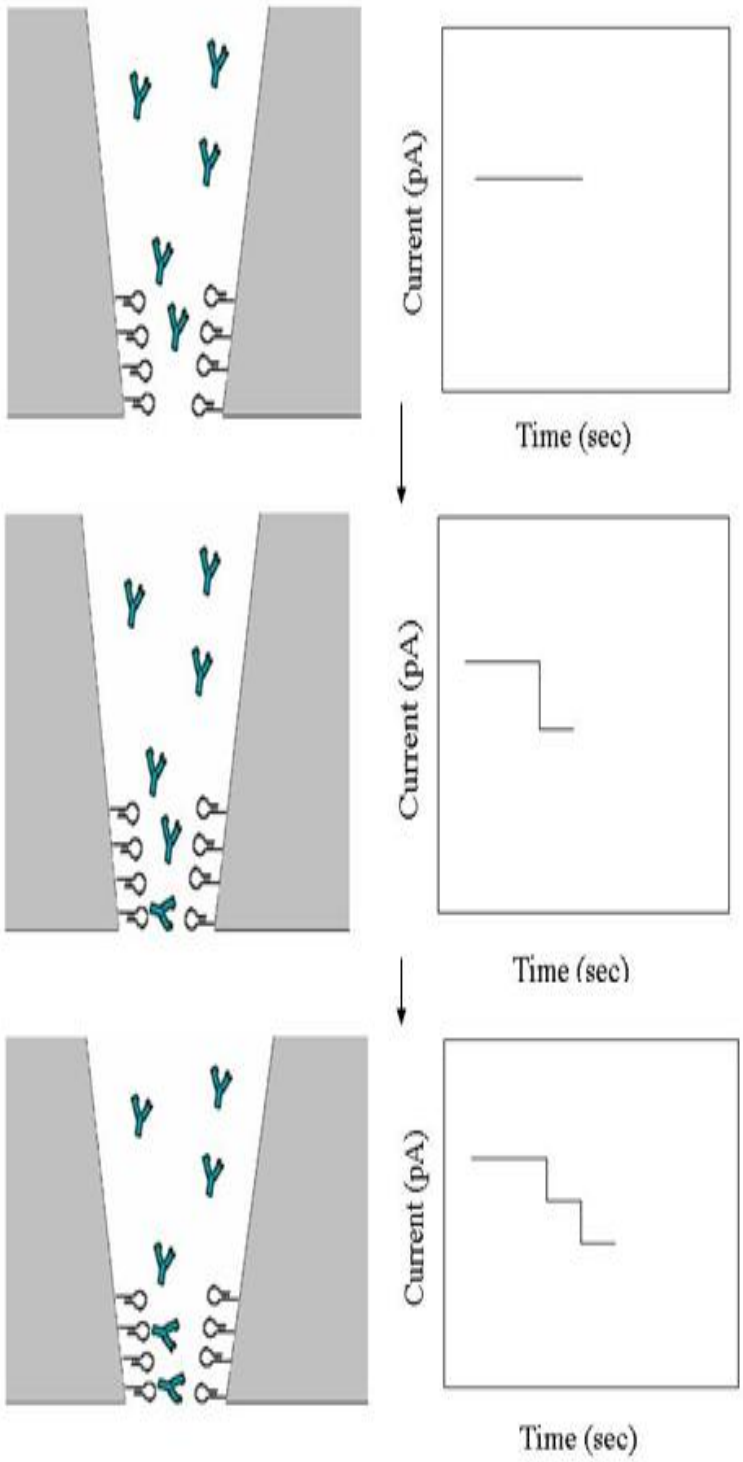

The lumen surface of the nanopore was coated with anti-IgE aptamers. Time-dependent current data were recorded when IgE molecules (5nM) were introduced into the nanopore. All the IgE detection experiments were carried out in a PBS solution (pH 7.4). Discrete binding events which are significant different from translocation events noticed in non-coated nanopore, were observed (Fig. 4.6). The current level was reduced step by step. The average event duration is 3.1mins and the current blockage level is 591pA. It took about 35 mins to eventually reach an equilibrium state, where the current is stable again at a permanently reduced level. Each discrete step indicates the dynamic process of single IgE molecule binding with anti-IgE aptamer. Because of the high affinity between the anti-IgE aptamer and the IgE molecule, the unbinding event was rarely observed.

Figure 4.6. IgE binding events.

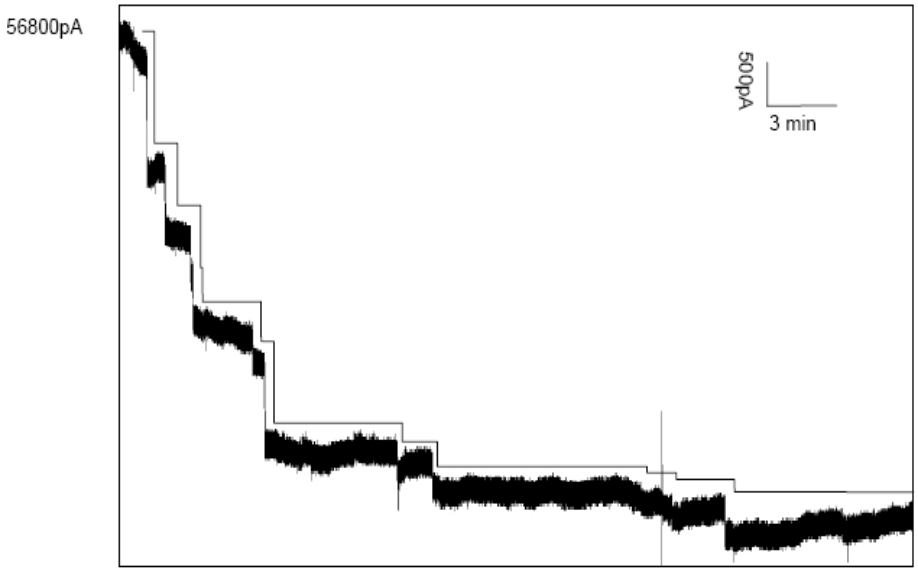

To verify the specific IgE binding, we did several control experiments, such as a nanopore without any aptamer modifications, with control-aptamer (a reversed sequence of anti-IgE aptamer), and with a mutant aptamer (a single base mutation). We didn't observe any non-specific protein absorption or IgE binding (Fig. 4.7).

Figure 4.7. Control experiments. non-coated, control aptamer and mutant aptamer coaded nanopore in presence of IgE (5nM) molecules.

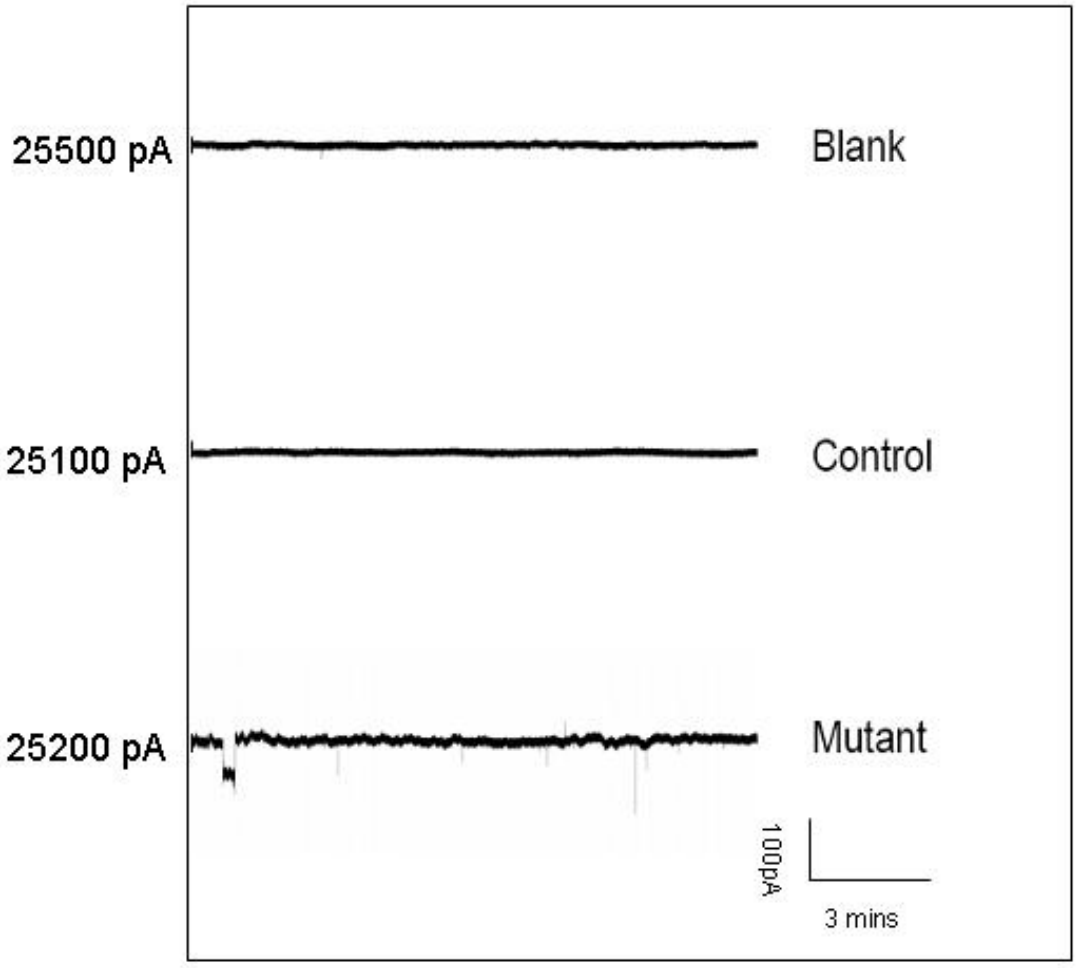

In addition, we incubated IgE with anti-IgE aptamer at a ratio of 1:10 to form the IgE-aptamer complex. Then we tested this IgE-aptamer complex with an anti-IgE aptamer coated nanopore. As expected, there was no IgE binding event (Fig. 4.8). Therefore, specific binding events can be only observed when IgE binds to anti-IgE aptamer.

Figure 4.8. IgE-aptamer complex in anti-IgE aptamer encoded nanopores.

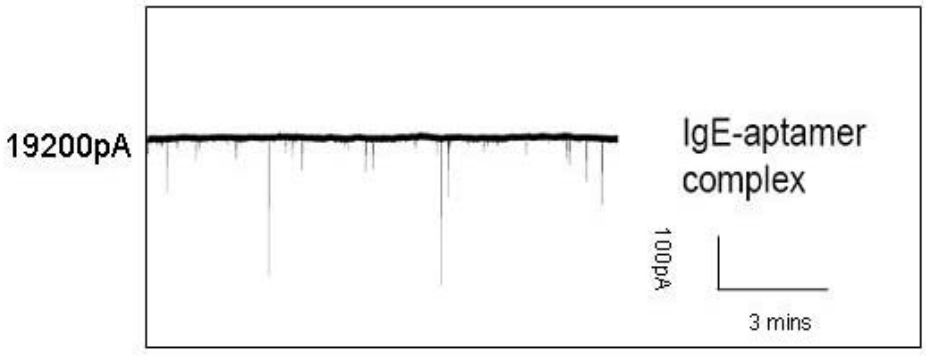

4.7 Selectivity of IgE detection

To investigate the selectivity of an anti-IgE aptamer coated nanopore towards its specific target, we tested it with IgG, which has a similar structure to IgE but is not recognized by the anti-IgE aptamer. We didn't detect any IgG binding event (Fig. 4.9). But after washing out IgG, we injected IgE into the same nanopore. Steplike binding events were observed again (Fig. 4.10). It verified the aptamer encoded nanopore is highly selective to its analyte and a specific binding event is able to be electrically detected.

Figure 4.9. IgG in anti-IgE aptamer encoded nanopores.

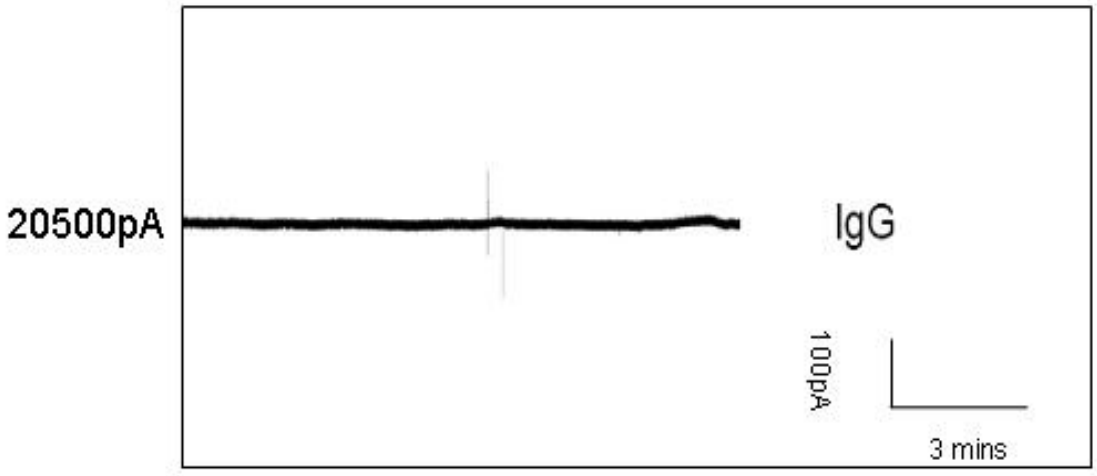

Figure 4.10. IgE detection after IgG test.

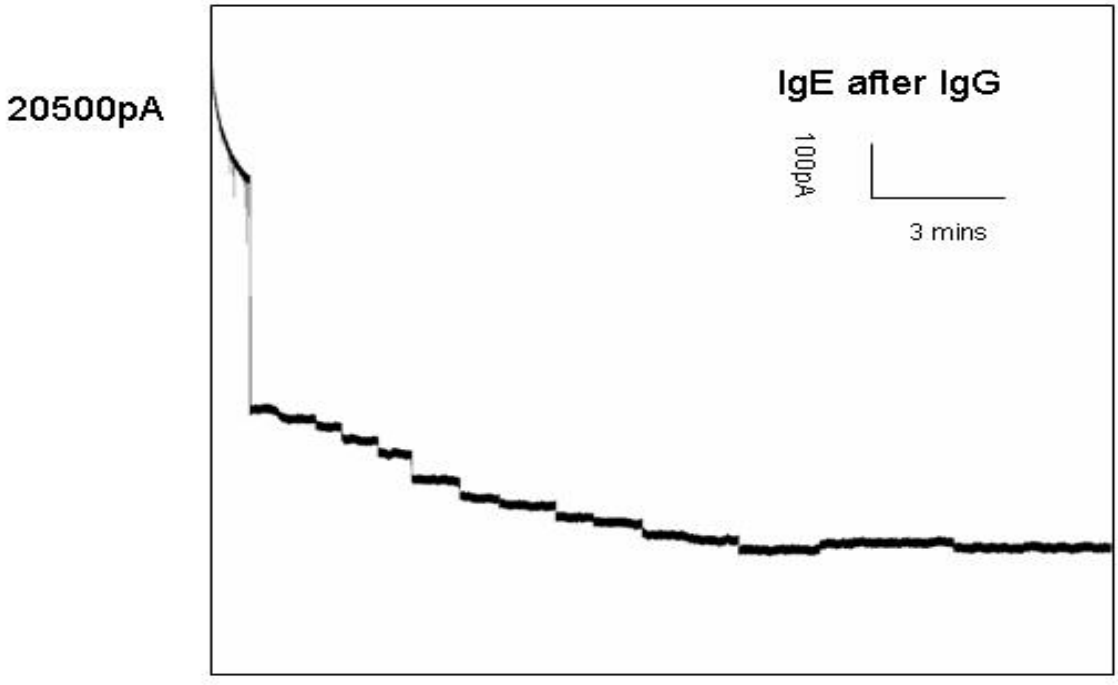

4.6 Releasing of captured IgE molecules

After IgE tightly bound with the aptamer, we introduced a restriction enzyme *(Hind*III) into the nanopore (Fig. 4.11). *Hind*III was used to make the permanent IgE binding reversible and to quantify the number of IgE detected by aptamers. When we chose an appropriate anti-IgE aptamer, a *Hind*III active site was designed to be inserted into the stem region of the anti-IgE aptamer, where the affinity of the aptamer was not influenced. After the IgE completely bound with the aptamer, we washed out the free IgE molecules and injected *Hind*III into the nanopore. Another type of events was captured immediately (Fig. 4.12). The current level was recovered in an upward step like pattern. The average release duration is 0.75 mins and the current recovery level is 208pA. We believe this is a *Hind*III cutting effect on the release of bound IgE. In theory, the current level should recover to its base line before the IgE binding. In fact, it recovered, but followed by shifting downward. This may be due to the *Hind*III diffusion, which is driven by the concentration gradient. When *Hind*III reaches the tip region, it will first recognize and bind onto the active site, and then cut the DNA aptamer. It is a fast process which happens in one minute. It is also a complicated dynamic phenomenon combined with *Hind*III binding and cutting effects. We observed that the current is first partially blocked and then recovered in steps.

Figure 4.11. Restriction enzyme *(Hind*III) binds and cuts DNA aptamer which is immobilized on the nanopore surface, and therefore releases the bounded IgE molecules.

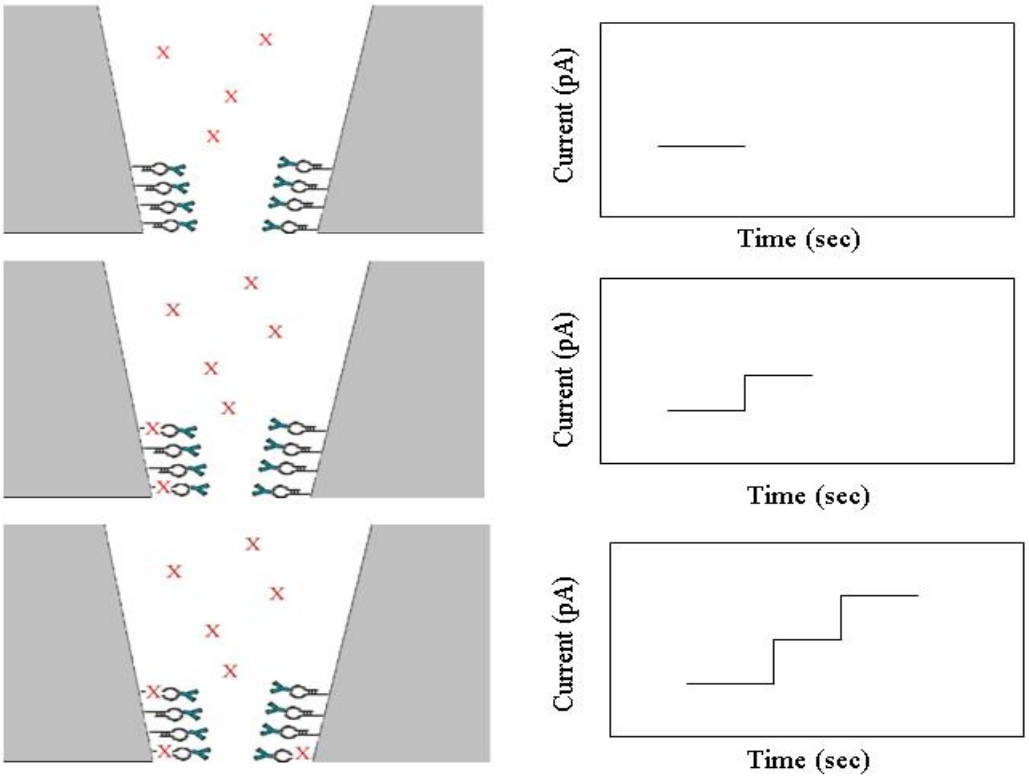

Figure 4.12. *Hind*III experiment recording (Current vs. Time).

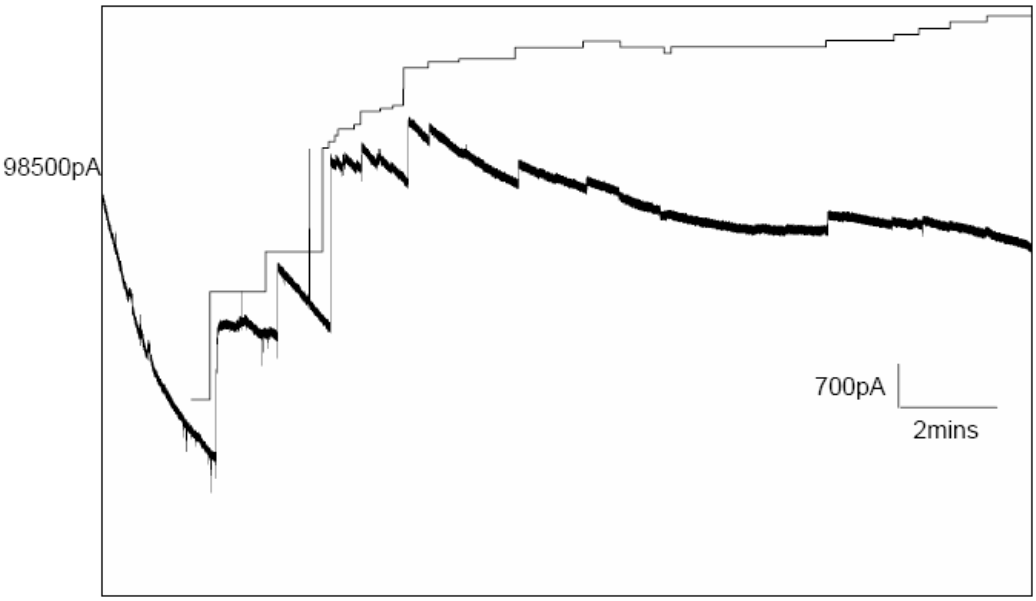

4.7 Sensitive IgE detection

The concentration dependent experiments were carried out to measure the time of the first binding event, which is mostly related to the IgE concentration. A minimum concentration is 500fM that can be detected in a reasonable time scale. We added IgE molecules in the external solution to eliminate the voltage effects (Fig. 4.13). The number of IgE molecules that enter the nanopore is both voltage and concentration dependent. The first binding time (τ_b) is the parameter that mostly relates to the concentration. While the IgE concentration decreases, it will take longer for the first IgE molecule to enter the nanopore and bind with the anti-IgE aptamer. As shown in Fig. 4.14, the first binding time (τ_b) increased when lowering the external IgE concentration. The variance is large in different concentration levels. It is possible that the stochastic sensing happened in a nanomolar concentration. However, the detection of IgE is highly sensitive. For example, it only takes about 4 minutes to detect an IgE molecule at 5nM.

Figure 4.13. Concentration dependent experiment setup.

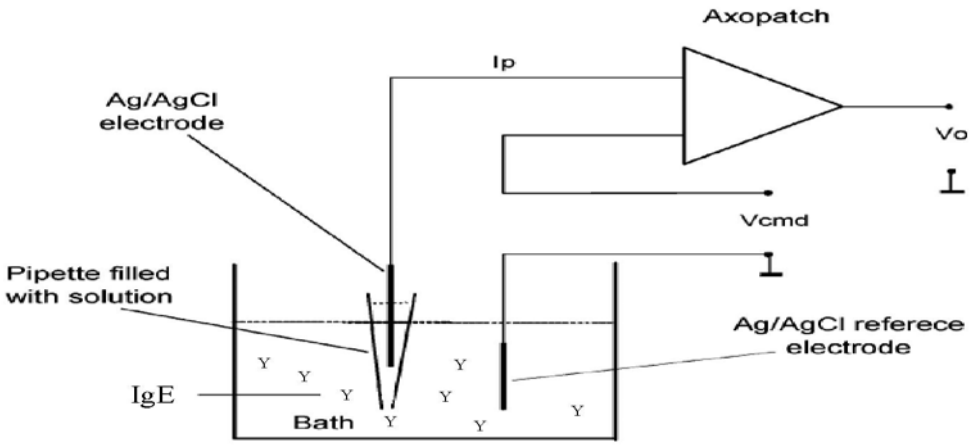

Figure 4.14. External IgE Concentration vs. First Binding Time.

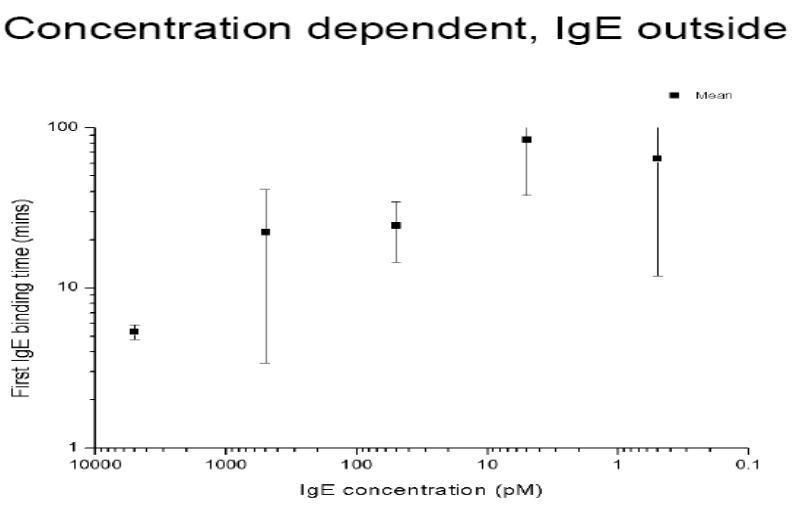

4.8 Single ricin detection

Ricin is a protein toxin that is extracted from the castor bean (Fig. 4.15). Ricin is poisonous if inhaled, injected, or ingested, acting as a toxin by the inhibition of protein synthesis. Ricin causes severe diarrhea and victims can die of shock. Ricin is one of the biothreat agents. Ricin has a great impact on biodefense.

Figure 4.15. Ricin structure (Weston et al., 1994).

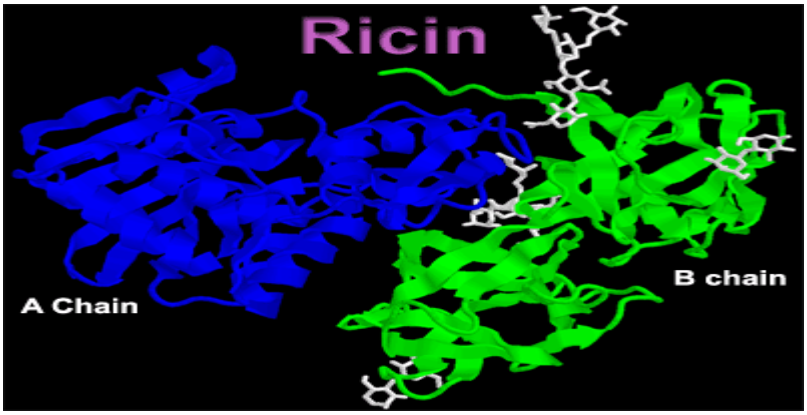

Like IgE detection experiments, we covalently linked anti-Ricin aptamers, which are RNA aptamers, onto the glass surface though the amino-group. Using the same electrical measurement as in IgE testing, single ricin molecules were rapidly detected at a very low concentration (Fig. 4.16). For example, the average time for detecting the first Ricin molecule in the external solution is about 5 minutes at 2.8 μM concentration. Even at 2.8nM, the average binding time is 32 minutes for detecting the first ricin molecule. Although the 2.8nM concentration is 1000 times smaller than 2.8μM, the detection is not slower in 1000 times. The results show the first binding time was dependent on the ricin concentration. However, the variation within each group is large, especially for 2.8nM. Because it is in such a low concentration, the stochastic detection is very random and it has a relatively low probability.

Figure 4.16. Ricin concentration dependent measurements.

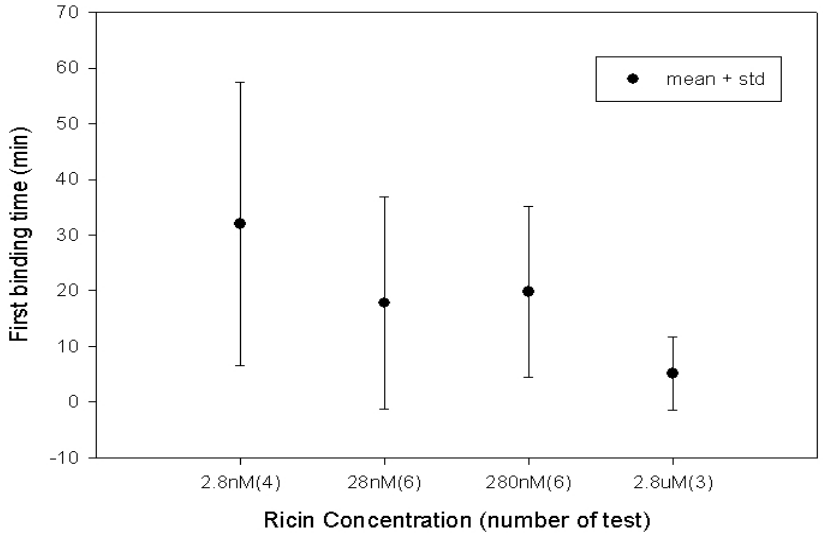

When ricin was presented in the external solution, the current base line was negative. Thus, ricin binding caused an upward current change (Fig. 4.17). The absolute value of the current was reduced or blocked. The average current block duration is 4.4mins and the amplitude blockage is 22.2pA. Here are two significant time periods during 2 hours of recording: fast phase (0-40 mins) and slow phase (40-120 mins).

Figure 4.17. The stochastic ricin detection.

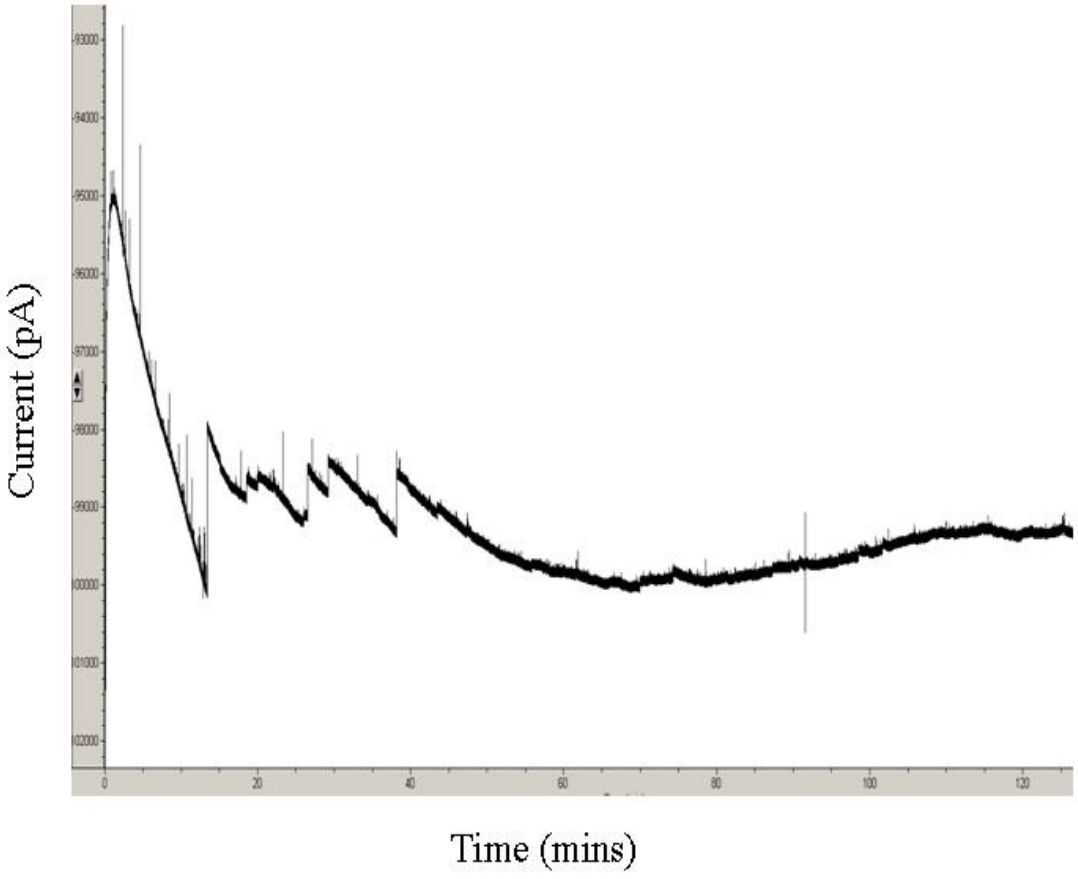

Conclusion

Our study shows that single IgE molecules can be detected directly with high selectivity in electrical measurement using the DNA aptamer functionalized glass nanopore. This is a great breakthrough in the single molecule level since this is the first time to specifically detect a single protein molecule using a solid-state nanopore. In addition, a single Ricin molecule was able to be detected in an RNA aptamer encoded nanopore, even at a low concentration. This demonstrated that using a glass nanopore as a biosensor could impact a single protein molecule detection for medical and biothreat applications.

CHAPTER 5

SINGLE ENZYME DYNAMICS

Objective

To study the enzyme molecule recognition and interaction at the single-molecule level, using an aptamer functionalized nanopore.

Methods

5.1 Streptavidin/biotin system and single enzyme kinetics

We designed a ssDNA with a biotin at the 5' end and an amino group at the 3' end. After hybridized with complementary DNA, this DNA was immobilized on the glass surface with a *Hind*III active site in the middle stem region. We detected the electrical signal of streptavidin binding to the biotin attached at the 5' end of DNA (Fig. 5.2). Then we examined the *Hind*III activity inside the functionalized nanopore, using the simple electrical measurement (Fig. 5.2).

Figure 5.1. A streptavidin/biotin system as a signal reporter.

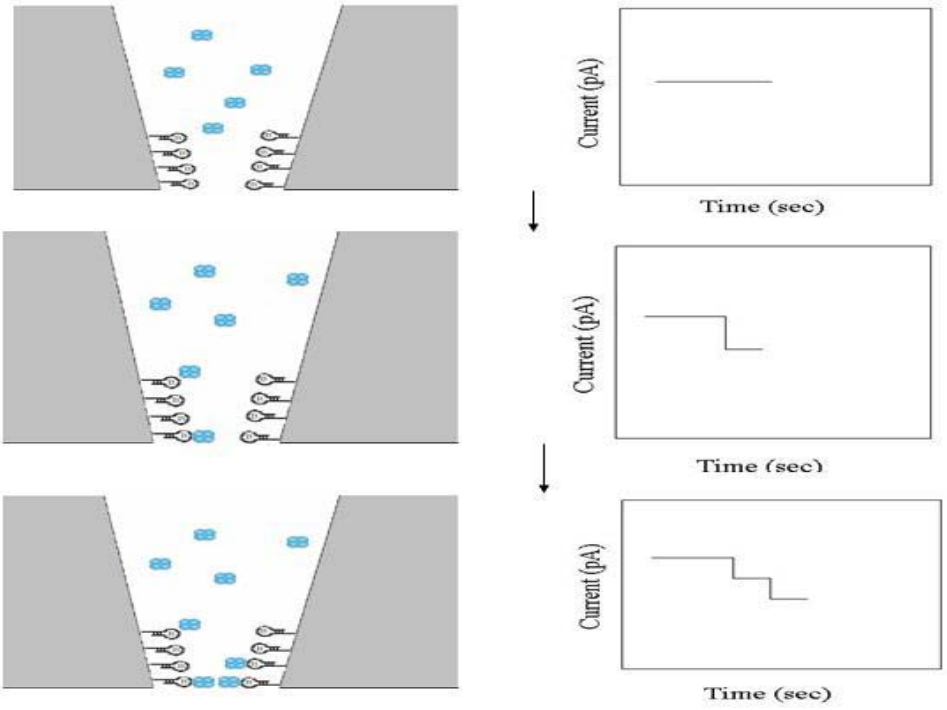

Figure 5.2. Single *Hind*III kinetics measurements in Streptavidin/biotin system.

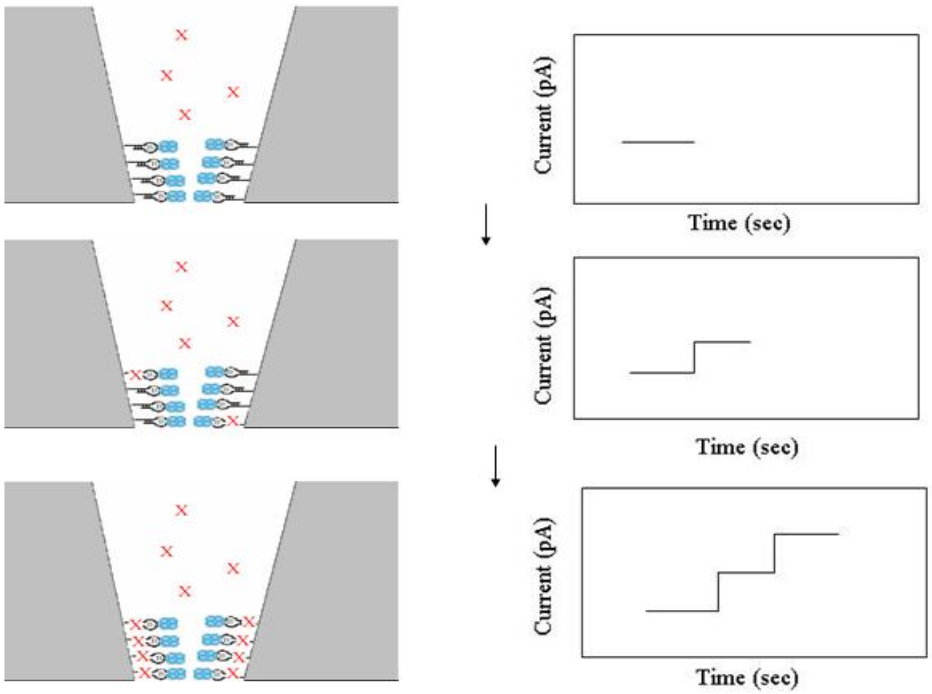

Results

5.2 Streptavidin and biotin

The streptavidin/biotin system is of special interest because it has one of the largest free energies of association for noncovalent binding of a protein and small ligand in aqueous solution. The complexes are also extremely stable over a wide range of temperature and pH.

Similar to the previous IgE and Ricin detection, the current was reduced in discrete steps after Streptavidin was introduced into the biotin linked nanopore (Fig. 5.3). The average block duration was 1.34 mins and block amplitude was 389pA.

Figure 5.3. Streptavidin bind to biotin.

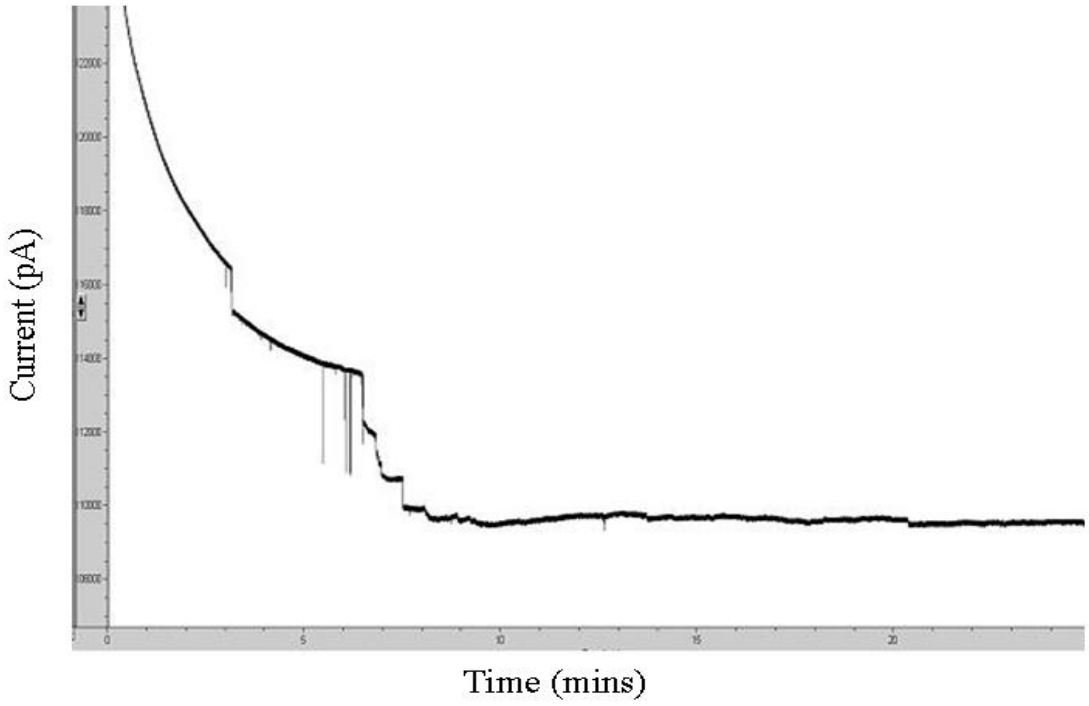

5.3 Single enzyme kinetics

Using the biotin/streptavidin as a reporter system, we observed the activity restriction enzyme (*Hind*III) at the single molecule level (Fig. 5.4). It showed clearly the single enzyme behavior in two different stages. The first stage (0-1 min) could be *Hind*III recognition. *Hind*III binds onto its active site and leads to a downward step-like current block. The average block duration was 0.125mins and block amplitude was 250pA.

The second stage (1-2 mins) could be *Hind*III cutting. It cuts the DNA and therefore releases the biotin/streptavidin. As the biotin/streptavidin leaves, the current recovers upward in steps. The average release duration was 0.07 mins and release amplitude was 143pA.

Figure 5.4. *Hind*III kinetics.

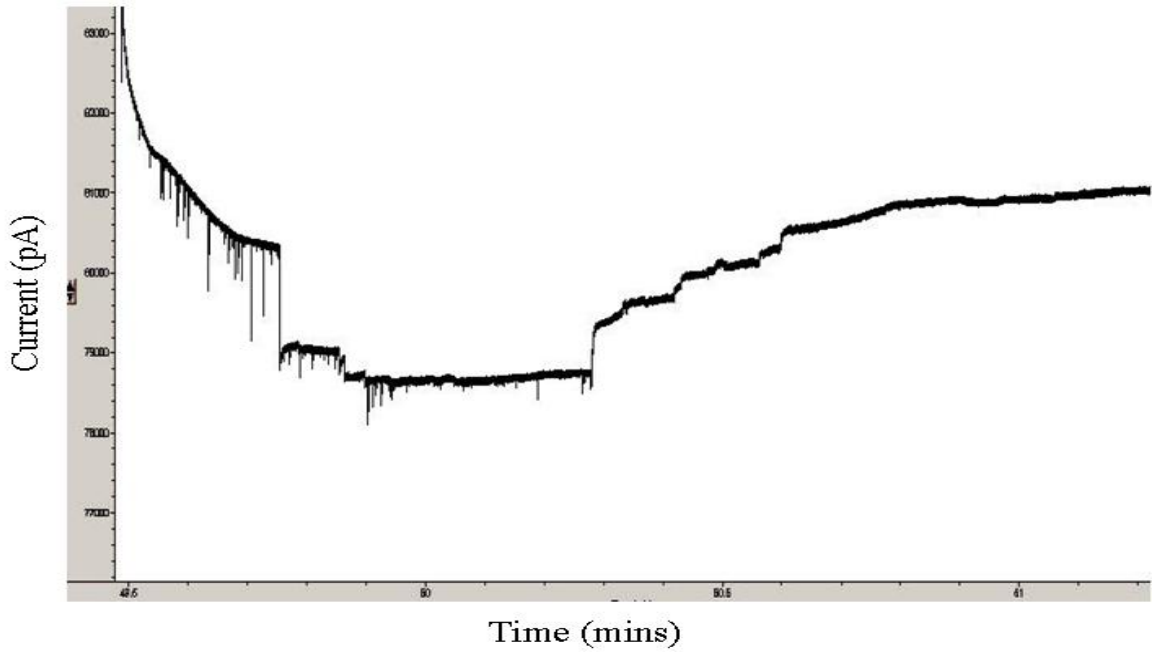

Conclusions

Glass nanopores achieved functions as biosensors, when DNA/RNAs were immobilized on the lumen surface. Although many detailed phenomenon were hard to explain, we have demonstrated the successful detection of specific targets, such as IgE, Ricin, and streptavidin/biotin with high sensitivity. One of the exciting observations is single enzyme activity within nano-confinement. The duration of the event could indicate the strength of the interaction and the amplitude of the event could indicate different protein conformations. We demonstrated the ability of functionalized nanopores to measure the interaction on a single molecule scale. It can provide deeper insight and understanding of the stochastic interaction of various biomolecules.

CHAPTER 6

FUTURE DIRECTION AND CONCLUSIONS

Applications

Because the pore can be made smaller than a molecule, it is possible to implant a single molecule into the pore to reveal the host-guest interaction such as screening synthesized libraries of cyclic peptides (Ghadiri et al., 1994) or exploring bio-processes, such as DNA digestion by the enzymatic ring-shaped motors (Vanoijen et al., 2003). Nanopores can also be made of special materials to achieve new properties, such as a pore with a hydrophobic lumen. Once filled with conductors such as gold, for example, the nanopore could become a molecular-scaled electrode for *in vivo* detection. Nanopores could also be used as atomic-scaled pens for the delivery of single molecules (Bruckbauer et al., 2002); and simultaneously observed optically to track single molecule processes (Harms et al., 2003).

A specific molecule binding event can be applied to investigate single molecule recognition and interaction. The ability of a functionalized nanopore can provide deeper insight and understanding of the stochastic interaction of various biomolecules.

For example, we have tested several anti-IgE aptamer mutations, such as C18T, C19T, C20T, deleted C18, C18-19 and C18-20, since we believe the hairpin loop structure of anti-IgE aptamer is the key domain which will interact with IgE strongly. We noticed that the molecule recognition behavior in mutant aptamer is different from wild type anti-IgE aptamer. We didn't observe any permanent IgE binding events in these mutations. There're only translocations or temporally binding events observed in these aptamer mutations. This gives us a sign that some small changes in aptamer structure may have a strong influence on the interaction between anti-IgE aptamer and analyte (IgE). It could be a good application in studying the single molecule recognition and detecting the mutation engineered molecules.

The simplicity, sensitivity and selectivity of aptamer modified nanopores suggest that it has a potential for integration into a useful single-molecule sensing device.

Conclusions

We have created a low noise, calibrated, molecular-scaled pore either by micro-forge polishing or externally penetrating a nanocavity enclosed in the sealed terminal of a micropipette. The nanopore fabrication is both cost-effective and time-efficient. The profile of the nanopore and the pore size-conductance correlation was determined. This work is significant both for the development of nanotechnologies and for understanding physical and chemical properties in a nano-confinement.

Our study shows that single IgE molecules can be detected directly with high selectivity in an electrical measurement using a DNA aptamer functionalized glass nanopore. This is a great breakthrough in the single molecule level, since this is the first time to specifically detect a single protein molecule using solid-state nanopore. In addition, a single Ricin molecule was able to be detected in RNA aptamer encoded nanopores even at a low concentration. This demonstrated glass nanopore as a biosensor could have an impact on single protein molecule detection for medical and biothreat applications.

Glass nanopores achieved functions as biosensors when DNA/RNAs were immobilized on the lumen surface. Although many detailed phenomenon were hard to explain, we have demonstrated the successful detection of specific targets, such as IgE, Ricin, and streptavidin/biotin with high sensitivity. One of the exciting observations is single enzyme activity within nano-confinement. The duration of the event could indicate the strength of the interaction and the amplitude of the event could indicate different protein conformations. We demonstrated the ability of functionalized nanopores to measure the interaction on a single molecule scale. It can provide deeper insight and understanding of the stochastic interaction of various biomolecules.

APPENDIX A

NANOPORE CHARACTERISTICS

Low noise

Nanopores constructed by either micro-forge or wet etching methods exhibit stable conductance and a low level of electrical noise. For example, after etching, we observed a current that was consistently flat, without drift and discrete change (Fig. A.1) for 20 mins. The noise level was comparable to that of α-hemolysin (αHL), a standard for low-noise protein nanopore systems. The current noise was measured using the value of IRMS displayed on the amplifier panel. The noise for this pore was 1.8 pA (1M NaCl, +200 mV), as low as that of αHL, which typically is 1.2-1.8 pA in the planar lipid bilayer under the same condition. Such a low noise level could be attributed to the external etching process, which minimizes the damage to the inside surface of the nanopore. The resulting clear background current is ideal for electrically addressing single-molecule block events.

Figure A.1. Nanopore electrical properties. a, low noise. b and c, current rectification.

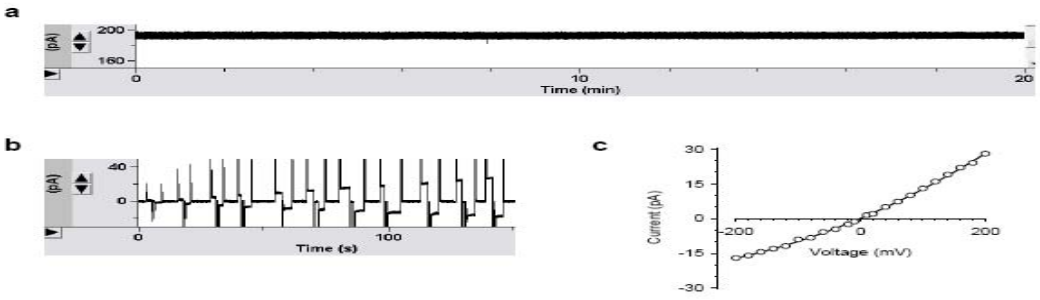

Current rectification

Measuring currents at different voltages, we found that this nanopore demonstrates a weakly rectified current-voltage relationship (I-V curve, Fig. A.1b and c). This could be a result of the asymmetrical pore shape and charged lumen. This rectification has also been found in pure water (ddI H2O) solution (Fig. A.2)

Figure A.2. Water effect (I-V curve). Voltage ramps from -1000mV to 1000mV.

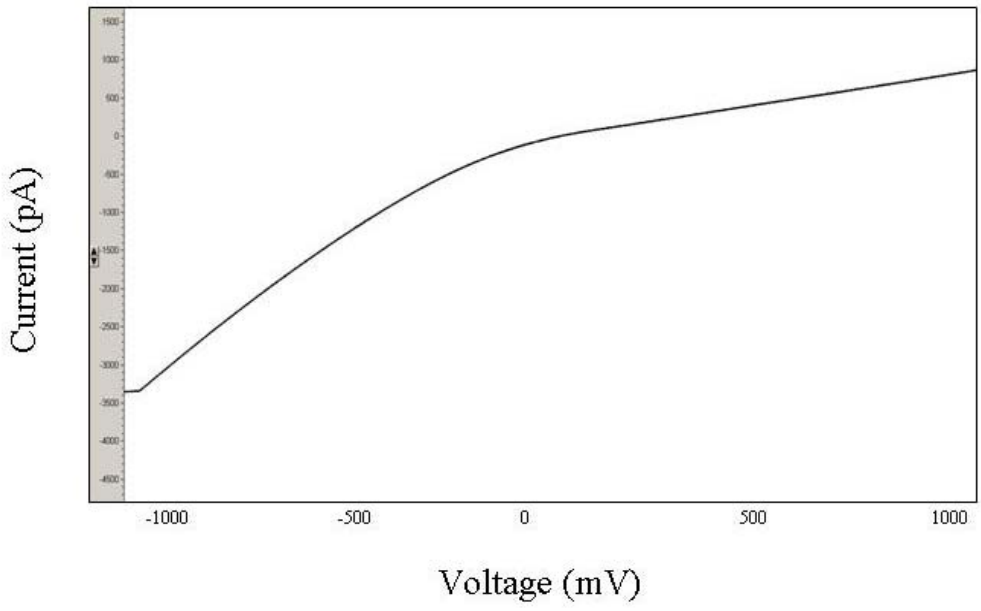

Tail current

When analytes (IgE or IgG) are presented in the nanopore without aptamer coating, the tail current is different from normal (Fig. A.3). At the positive voltage, it has a peak and drops fast. But at the negative voltage, it has two separate stages. One is fast and the other is slow. This tail current is voltage dependent (Fig. A.4).

Stability

The glass nanopore is highly stable under various conditions. It's portable and reusable after 24 hours or even longer time recording.

Figure A.3. Tail currents in positive and negative voltage.

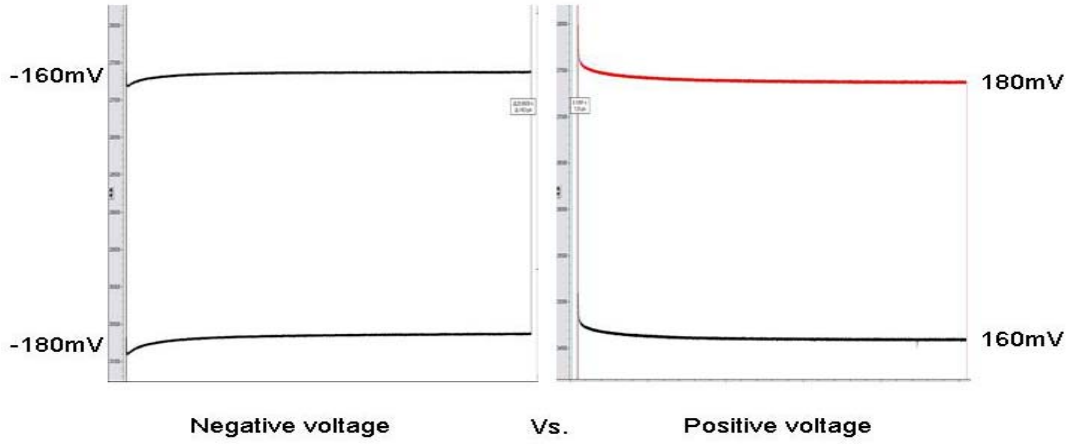

Figure A.4. Voltage dependent tail currents.

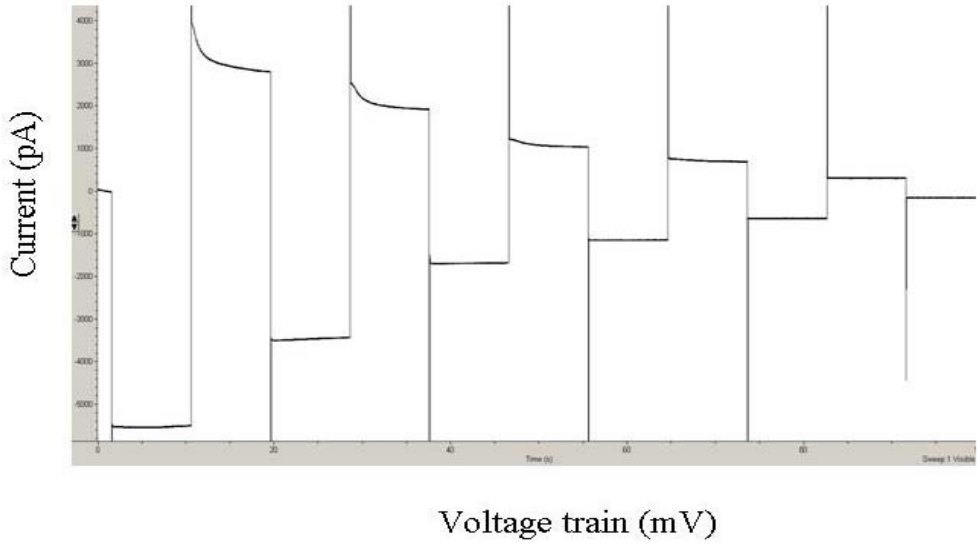

APPENDIX B

METHODS AND INSTRUMENTATION

Chemicals

An Au-NP with a diameter of 10 nm was purchased from Ted Pella Inc. According to the company, the sample contained 5.7×1012 particles/ml (~9.5 nM) with a coefficient of size variation < 8%. Au-NP was diluted to 4.75 nM in 15 mM NaCl for translocation experiments. A fresh nanoparticle preparation was used for each test. In order to confirm no aggregation in the low salt concentration, 300 μl samples of 4.75 Nm Au-NP in a 15 mM NaCl solution and in pure water (control) were analyzed using a DynaPro99 Molecular Size Instrument (Dynamic Light Scattering) to obtain the particle size distribution. The 1.0 kbp dsDNA originated from the 4.45 kbp plasmid DNA pT7- αHL, which was digested with *Hind*III and *Nde*I restrictive endonucleases overnight, separated on an agarose gel and purified with the DNA purification kit (QiaGen). The purified 1.0 kbp ds-DNA was 22 ng/μl and diluted to 10 nM in a 1 M NaCl solution. PCR was performed with the Polymer Chain Reaction (PCR) kit (Roche Corporate) using a Robocycler PCR instrument (Stratagene Inc). The primers for DNA amplification were synthesized and purified by Integrated DNA Technologies Inc. The sequences of the forward and backward primers were 5'-AGTGGTTTAGCCTGGCCTTC-3' and 5'- TCTTGGAACCCGGTATATGG-3'. The PCR product between the two primers was 350 base pairs and was examined on the agarose gel. The (R)-(+)-ibuprofen was purchased from Toronto Research

Company (Canada); cyclodextrins and other chiral enantiomers were purchased from Sigma-Aldrich.

IgE (purified from Human Myeloma Plasma, Kappa) and IgG (purified from Human Plasma), with purity greater than 95% by SDS-PAGE, were purchased from Athern Research & Technology (Athens GA 30604). Aptamers, 3'-modified with amino groups (3' Amino Modifier), were obtained from IDT Integrated DNA Technologies, Inc.

Anti-IgE aptamer is a DNA aptamer which has a hairpin loop and a stem region: (Fig.) 5' - GGG GCA CGT TTA TCC GTC CCT CCT AGT GGC GTG CCC C/3AmM/ - 3' (HPLC Purification, 37 bases)

Control aptamer: 5' - CCC CGT GCG GTG ATC CTC CCT GCC TAT TTG CAC GGG G/3AmM/ - 3' (HPLC Purification, 37 bases)

Anti-IgE aptamer with *Hind*III active site: 5'-modified with amino groups (5' Amino Modifier C6) 5' - /5AmMC6/CCC AAG CTT GGG AAA GGG GCA CGT TTA TCC GTC CCT CCT AGT GGC GTG CCC CTT TCC CAA GCT TGG G - 3' (100 nmole DNA oligo, HPLC Purification, 67 bases)

Nanopore fabrication and electrical measurement

Before use, the borosilicate glass tube (1.5 mm o.d. and 0.86 mm i.d.) with an inner filament (A-M System Inc.) was washed with ethanol and double deionized water (ddH2O), followed by drying in nitrogen air.

Recording solutions. In the DNA translocation experiment, both internal and external solutions contained 1 M NaCl. A 10nM DNA was presented in the external solution. All solutions were buffered with 10 mM Tris and titrated to pH7.2.

Pico-ampere electrical recording and data analysis. Conductance was measured using an Axopatch 200B-2 patch-clamp amplifier (Molecular Device Inc.), then low-pass filtered with a built-in 4-pole Bessel filter at 1-5 kHz and sampled at 5-10 kHz with a Digidata 1332 A/D converter (Molecular Device Inc.). For all measurements, the external solution was grounded as the convention for voltage polarity. Current amplitudes and durations of single molecule block events were obtained from histograms constructed using pClamp software (Molecular Device Inc.). The amplitudes were obtained by fitting the amplitude peaks to Gaussian functions or averaging the amplitudes of measured block events. Block durations (τ) and rates (f) were obtained from the arithmetic mean of total block events (the low number of events). The DNA translocation rate constant was calculated by kon = f /[DNA], where [DNA] is the DNA concentration and the rate

REFERENCES

Bruckbauer, A., Ying, L., Rothery, A. M., Zhou, D., Shevchuk, A. I., Abell, C., Korchev, Y. E., and Klenerman, D. 2002. Writing with DNA and protein using a nanopipet for controlled delivery. *J. Am. Chem. Soc.* 124, 8810-11.

Chang, H., Kosari, F., Andreadakis, G., Alam, M. A., Vasmatzis, G., and Bashir, R. 2004. DNA-mediated fluctuations in ionic current through silicon oxide nanopore channels. *Nano Letters* 4, 1551-56.

Cho, E. J., Collett, J. R., Szafranska, A. E., and Ellington, A. D. 2006. Optimization of aptamer microarray technology for multiple protein targets. *Analytical Methods for Proteomics* 564, 82-90.

Dekker, C. 2007. Solid-state nanopore. *Nature Nanotechnology* 2, 209-15.

Gao, C., Ding, S., Tan, Q., and Gu. L. 2008. A simple method of creating a nanopore-terminated probe for single-molecule enantiomer discrimination. *Analytical Chemistry* (Accepted).

Ghadiri, M. R., Granja, J. R., and Buehler, L. K. 1994. Artificial transmembrane ion channels from self-assembling peptide nanotubes. *Nature* 369, 301-4.

Gould, H. 2003. The biology of IGE and the basis of allergic disease. *Annu. Rev. Immunol.* 21, 579-628.

Harrell, C. C., Choi, Y., Horne, L. P., Baker, L. A., Siwy, Z. S., and Martin, C. R. 2006. Resistive-pulse DNA detection with a conical nanopore sensor. *Langmuir* 22, 10837-43.

Harms, G. S., Orr, G., Montal, M., Thrall, B. D., Colson, S. D., and Lu, H. P. 2003. Probing conformational changes of gramicidin ion channels by single-molecule patch-clamp fluorescence microscopy. *Biophysical Journal* 85, 1826-38.

Howorka, S., Cheley, S., and Bayley, H. 2001. Sequence-specific detection of individual DNA strands using engineered nanopores. *Nature Biotechnology* 19, 636-9.

Kasianowicz, J., Brandin E., Braton D., and Deamer, D. W. 1996. Characterization of individual polynucleotide molecules using a membrane channel. *Proc. Natl Acad. Sci. USA* 93, 13770-3.

Li, J., Stein, D., McMullan, C., Branton, D., Aziz, M. J., and Golovchenko, J. A. 2001. Ion-beam sculpting at nanometre length scales. *Nature* 412, 166-9.

Samir M. I., Akin D., and Bashir, R. 2007. Solid-state nanopore channels with DNA selectivity. *Nature Nanotechnology* 2, 243-8.

Song, L., Hobaugh M. R., Shustak C., Cheley S., Bayley H., Gouaux, J. E. 1996. Structure of staphylococcal alpha-hemolysin, a heptameric transmembrane pore. *Science* 274, 1859-66.

Stadther K., Wolf H., and Lingner, P. 2005. An aptamer-based protein biochip. *Anal. Chem.* 77, 3437-43.

Storm, A. J., Chen J. H., Ling X. S., Zandbergen H. W., and Dekker, C. 2003. Fabrication of solid-state nanopores with single-nanometre precision. *Nature Mater.* 2, 537–40.

Storm, A. J., Chen J. H., Zandbergen, H. W., and Dekker, C. 2005. Translocation of double-strand DNA through a silicon oxide nanopore. *Phys. Rev. E* 71, 051903.

Vanoijen, A. M., Blainey, P. C., Crampton, D. J., Richardson, C. C., Ellenberger, T., and Xie, X. S. 2003. Single-molecule kinetics of λexonuclease reveal base dependence and dynamic disorder. *Science* 301, 1235-8.

Weston, S.A., Tucker, A.D., and Thatcher, D.R. 1994. X-ray structure of recombinant ricin A-chain at 1.8 A resolution. *J. Mol. Biol.* 244, 410-22.